Monthly Notices
of the
ROYAL ASTRONOMICAL SOCIETY

MNRAS **462,** S253–S273 (2016) doi:10.1093/mnras/stw2601
Advance Access publication 2016 October 8

Sulphur-bearing species in the coma of comet 67P/Churyumov–Gerasimenko

U. Calmonte,[1]★ K. Altwegg,[1,2]★ H. Balsiger,[1] J. J. Berthelier,[3] A. Bieler,[1,4] G. Cessateur,[5] F. Dhooghe,[5] E. F. van Dishoeck,[6] B. Fiethe,[7] S. A. Fuselier,[8] S. Gasc,[1] T. I. Gombosi,[3] M. Hässig,[1,8] L. Le Roy,[1] M. Rubin,[1]★ T. Sémon,[1] C.-Y. Tzou[1] and S. F. Wampfler[2]

[1]*Physikalisches Institut, University of Bern, Sidlerstrasse 5, CH-3012 Bern, Switzerland*
[2]*Center for Space and Habitability, University of Bern, Sidlerstrasse 5, CH-3012 Bern, Switzerland*
[3]*LATMOS, 4 Avenue de Neptune F-94100 Saint-Maur, France*
[4]*Climate and Space Sciences and Engineering, University of Michigan, Ann Arbor, MI 48109, USA*
[5]*Royal Belgian Institute for Space Aeronomy (BIRA-IASB), Ringlaan 3, B-1180 Brussels, Belgium*
[6]*Leiden Observatory, Leiden University, PO Box 9513, NL-2300 RA Leiden, the Netherlands*
[7]*Institute of Computer and Network Engineering (IDA), TU Braunschweig, Hans-Sommer-Strasse 66, D-38106 Braunschweig, Germany*
[8]*Space Science Division, Southwest Research Institute, 6220 Culebra Road, San Antonio, TX 78228, USA*

Accepted 2016 October 5. Received 2016 October 5; in original form 2016 June 29

ABSTRACT

Several sulphur-bearing species have already been observed in different families of comets. However, the knowledge on the minor sulphur species is still limited. The comet's sulphur inventory is closely linked to the pre-solar cloud and holds important clues to the degree of reprocessing of the material in the solar nebula and during comet accretion. Sulphur in pre-solar clouds is highly depleted, which is quite puzzling as the S/O ratio in the diffuse interstellar medium is cosmic. This work focuses on the abundance of the previously known species H_2S, OCS, SO, S_2, SO_2 and CS_2 in the coma of comet 67P/Churyumov–Gerasimenko measured by *Rosetta* Orbiter Spectrometer for Ion and Neutral Analysis/Double Focusing Mass Spectrometer between equinox and perihelion 2015. Furthermore, we present the first detection of S_3, S_4, CH_3SH and C_2H_6S in a comet, and we determine the elemental abundance of S/O in the bulk ice of $(1.47 \pm 0.05) \times 10^{-2}$. We show that SO is present in the coma originating from the nucleus, but not CS in the case of 67P, and for the first time establish that S_2 is present in a volatile and a refractory phase. The derived total elemental sulphur abundance of 67P is in agreement with solar photospheric elemental abundances and shows no sulphur depletion as reported for dense interstellar clouds. Also the presence of S_2 at heliocentric distances larger than 3 au indicates that sulphur-bearing species have been processed by radiolysis in the pre-solar cloud and that at least some of the ice from this cloud has survived in comets up the present.

Key words: space vehicles – space vehicles: instruments – comets: general – comets: individual: 67P/Churyumov–Gerasimenko.

1 INTRODUCTION

Comets are thought to represent a link between the interstellar dense cloud from which the solar nebula and then the Sun and planets formed, and today's Solar system. Cometary material is thought to contain material from the interstellar dense cloud, which has been reprocessed during Solar system formation. The discussion of the degree of reprocessing ranges from more or less unprocessed material to complete dissociation and formation in the solar nebula. By studying the volatile material of comets, we can try to assess how pristine cometary material is and from there obtain boundary conditions for the formation of planetesimals and their history in the Solar system.

The rich sulphur chemistry observed in comets and in pre-solar clouds is especially suited to test several hypotheses on the degree of reprocessing of cometary material prior to its incorporation into comets. Sulphur is the 10th most abundant element in

★ E-mail: ursina.calmonte@space.unibe.ch (UC); kathrin.altwegg@space.unibe.ch (KA); martin.rubin@space.unibe.ch (MR)

the universe. Organic sulphur chemistry resembles oxygen chemistry. Many molecules are very similar just exchanging oxygen by sulphur like e.g. formaldehyde (H_2CO) and thioformaldehyde (H_2CS). It is therefore interesting to look for these organo-sulphur species in the cometary coma. However, due to its ability to exist in the form of many allotropes, second only to carbon, sulphur is much more versatile and is found in very different molecules, starting from the polar H_2S to the stable, refractory ring molecule S_8. In dense clouds and star-forming regions, sulphur seems to be highly depleted by about a factor of 1000 relative to its cosmic abundance (Penzias et al. 1971; Tieftrunk et al. 1994) whereas in the diffuse interstellar medium (ISM) it is present with its cosmic abundance relative to oxygen of ∼1/37 (Savage & Sembach 1996; García-Rojas et al. 2006; Howk, Sembach & Savage 2006; Jenkins 2009).

Many papers have addressed this interstellar sulphur puzzle (see Woods et al. 2015 and references therein). Gas-phase sulphur chemistry requires at least one endothermic reaction for the formation of the corresponding hydride (van Dishoeck & Blake 1998). It is therefore commonly thought that grain surface chemistry plays an important role in the formation of sulphur-bearing molecules, as it does in the formation of water. Atomic sulphur may have been frozen out on to dust grains, where it is hydrogenated to form H_2S. However, H_2S is not detected in the ice in cold clouds at levels of $H_2S/H_2O < 3$ per cent (van der Tak et al. 2003), with even more stringent limits down to 0.2 per cent given by Jiménez-Escobar & Muñoz Caro (2011). These limits are clearly lower than the overall S/O ratio of 1/37. The detection of S_2 in comet C/1983 H1 *IRAS*–Araki–Alcock (A'Hearn, Schleicher & Feldman 1983) then led to the hypothesis that H_2S is destroyed in water-rich grain mantles by UV photons, X-rays or cosmic rays (i.e. highly energetic ions, also denoted as radiolysis; e.g. Grim & Greenberg 1987; Moore, Hudson & Carlson 2007). A large suite of ice processing experiments have been performed, showing that H_2S can indeed be transformed into other molecules such as OCS and S_2 in the ice. In addition, a more refractory component containing larger S-polymers up to S_8 and complex species such as hexathiepan (S_6CH_2) is produced as well when the ice is heated (e.g. Ferrante et al. 2008; Jiménez-Escobar & Muñoz Caro 2011). The products depend on the initial ice composition, as illustrated in recent experiments (e.g. Garozzo et al. 2010; Chen et al. 2015). Note that OCS can potentially also be formed by low-temperature surface reactions of CO with S without the need for photolysis or radiolysis.

The only detected interstellar ices containing sulphur in cold clouds are OCS (Palumbo, Geballe & Tielens 1997) and SO_2 (Boogert et al. 1997; Zasowski et al. 2009) but their abundances of (0.03–0.16) per cent and (0.2–1) per cent with respect to water ice are not enough to account for all of the sulphur. CS_2 may be expected to be the result of photolysis of H_2S ice, but this molecule has also not yet been detected in interstellar ices. Gas-phase observations have identified various sulphur-bearing molecules in protostellar sources ('hot cores') where ices have just sublimated off the grains. Many simple molecules like CS, SO, SO_2, H_2S, H_2CS, OCS, NS and others are routinely detected (e.g. Blake et al. 1994; Hatchell et al. 1998; van der Tak et al. 2003; Herpin et al. 2009; Crockett et al. 2014), but other species expected from H_2S processing like S_2, HS_2 and H_2S_2 are not (see Martín-Doménech et al. 2016 and references therein). Again, the total abundances of sulphur-bearing molecules fall below the expected S/O ratio.

For the gas coma of comet C/1995 O1 Hale–Bopp, a S/O ratio 0.02 has been reported (Bockelée-Morvan et al. 2000). This is 23 per cent below the photospheric value reported of 0.0257 ± 0.0018 (Lodders 2010). Since no information on the uncertainty of the Hale–Bopp measurement is provided, it is assumed to be ±0.01. Then, the minimal S/O value of 0.01 for the gas coma of Hale–Bopp would still be above the degree of the depleted elemental abundance S/O seen in dense clouds and star-forming regions.

A major goal of this paper is therefore the question if comets lack sulphur as well as it seems to be the case for dense pre-solar clouds, or if this lack of sulphur is indeed just an observational bias by remote sensing, not being able to detect the refractory sulphur produced by photolysis and radiolysis on grain surfaces.

In the Solar system, sulphur is abundant on many planets and their moons. Sulphur dioxide (Toon, Pollack & Whitten 1982) and atomic sulphur S, S_2, S_3, S_4 up to S_8 (Esposito, Winick & Stewart 1979) give a reddish colour to Venus' fumes. The volcanoes on the Jupiter moon Io also shed sulphur in the form mostly of SO_2 (Pearl et al. 1979) as of course do the volcanoes on Earth. Jupiter has a very interesting sulphur chemistry in its plasmasphere (Huddleston et al. 1998) mostly from ionized sulphur species supplied by Io. Some of the reddish colour on Jupiter may also be due to S_8. It seems that in Jupiter all heavy elements are enhanced compared to their solar value. For sulphur, this enhancement factor is up to 2.5 (Atreya et al. 2003). This enhancement is discussed as being the result of a cold environment at the location where Jupiter was formed. The most plausible hypothesis is an extremely low temperature (less than 30 K) of the planetesimals which trapped and supplied the volatiles containing the heavy elements to Jupiter (Owen et al. 1999). The scenario by Gautier et al. (2001) is an alternate hypothesis which relies on the trapping of volatiles containing the heavy elements in clathrate hydrates in the cooling feeding zone of Jupiter to explain their high abundance. This hypothesis overestimates the sulphur abundance in Jupiter by a factor of 2. Pasek et al. (2005) claim that sulphur chemistry in the solar nebula cannot be looked at in isolation rather it must be considered together with the abundance of water vapour. This condition very much depends on whether the chemistry takes place inside or outside the water snow line. All these observations make sulphur and its chemistry a very important topic to study in comets as they can give a clue on the mysterious sulphur depletion in star-forming regions as well as on the formation scenarios of the giant planets.

In 1980, the first detection of sulphur species in a cometary coma was reported, namely the radicals S and CS in comet C/1975 West (Smith, Stecher & Casswell 1980). Since then, many more sulphur-bearing species like SO, SO_2, OCS, CS_2, H_2S and S_2 (see Table 1) have been added pointing to a complex sulphur chemistry in comets. Hydrogen sulphide (H_2S) is the major sulphur-bearing species in comets including 67P/Churyumov–Gerasimenko. Prior to *Rosetta*, only comet Hale–Bopp has been bright enough to detect all of the above species in one comet.

Following the definition of Cottin & Fray (2008), there are three possible sources for molecules and radicals measured in the cometary coma: a nucleus source, parent molecules directly released from the subsurface ice of the nucleus, a secondary source for daughter species, which is due to the photodissociation of parent molecules in the coma or by chemical reactions in the coma, and a distributed source which is due to volatiles and semi-volatiles sublimating from dust grains or the thermal degradation of dust grains in the coma. Remote sensing is especially sensitive to the radicals SO, S and CS but it is not clear whether they are only daughter species from secondary sources or if they are also present as parent molecules. This question can be answered by direct *in situ* mass spectrometry.

Shortly after the arrival of *Rosetta* in the close vicinity of 67P/Churyumov–Gerasimenko (hereafter 67P), still at large

Table 1. Abundance of S-bearing species relative to water. This table is based on table 1 in Rodgers & Charnley (2006) and on table 1 in Bockelée-Morvan et al. (2004a). Please note that most of these values come from remote sensing measurements, for which CS is assumed to be the photodissociation product of CS_2.

Molecule	67P/Churyumov–Gerasimenko (3.15 au, summer–winter)	C/1995 O1 Hale–Bopp (∼1 au)	C/2014/Q2 Lovejoy (∼1 au)	Other comets (see Table A2) (0.46–4.76 au)
H_2S	0.0067–0.0175[22]	0.015[14]	0.005[23]	0.0013–0.0115[2, 4, 5, 8–11, 19–21]
OCS	0.000 17–0.000 98[22]	0.004[14]–0.0046[13]	0.000 34[23]	0.001–0.0028[4, 12, 13, 16, 28]
SO	0.000 04–0.000 014[22]	0.0026–0.0041[14]	0.000 38[23]	0.0011–0.0028[14, 19]
SO_2	0.000 11–0.000 41[22]	0.0015–0.0021[14]	–	–
CS	a)	0.0040–0.01[7]	0.000 43[23]	0.000 08–0.006[1–4, 6, 8, 17, 19–21, 26]
CS_2	0.000 03–0.000 24[22]	–	–	–
H_2CS	–	0.0005[24]	0.000 13[23]	–
S_2	0.000 004–0.000 013[22]	–	–	0.000 012–0.0002[1, 16–18, 25, 27]
NS	–	≥0.0002[15]	0.000 06[23]	–

[1]Kim & A'Hearn (1991); [2]Biver et al. (1999); [3]Wouterloot et al. (1998); [4]Biver et al. (2000);
[5]Bockelée-Morvan et al. (2001); [6]Weaver et al. (1999); [7]Snyder et al. (2001); [8]Bockelée-Morvan et al. (2004b);
[9]Eberhardt et al. (1994); [10]Biver et al. (2002); [11]Crovisier et al. (1991); [12]Woodney, McMullin & A'Hearn (1997);
[13]Dello Russo et al. (1998); [14]Bockelée-Morvan et al. (2000); [15]Irvine et al. (2000);
[16]Bockelée-Morvan et al. (2004a); [17]Weaver et al. (2002); [18]Feldman et al. (1999); [19]Biver et al. (2006);
[20]Biver et al. (2008); [21]Biver et al. (2007); [22]Le Roy et al. (2015); [23]Biver et al. (2015); [24]Woodney (2000);
[25]Weaver et al. (1996); [26]Meier & A'Hearn (1997); [27]Weaver (2000); [28]Dello Russo et al. (2016).
Comments: a) CS cannot be resolved from CO_2 by ROSINA for these specific measurements.
[14]Abundances relative to water are computed assuming [HCN]/[H2O]=2.5E−3.
[20]Please note that the values have been determined graphically.

heliocentric distances (above 3 au), all of the above sulphur-bearing species were found by ROSINA (*Rosetta* Orbiter Spectrometer for Ion and Neutral Analysis; Balsiger et al. 2007) in the coma of the Jupiter-family comet. The measurements in 67P at a distance of 3.15 au from the Sun (Le Roy et al. 2015) are listed in Table 1 with two different values corresponding to the Northern (summer) and Southern (winter) hemispheres. Except SO, the abundances of S-bearing species relative to water were a factor of 3–8 higher above the winter compared to the summer hemisphere. SO/H_2S on the other hand is about a factor of 3 lower above the winter with respect to the summer hemisphere. These measurements were done outside of the water snow line and thus abundances relative to water are not expected to be representative of the bulk composition. The two hemispheres at that heliocentric distance showed a very heterogeneous coma with water coming mainly from the northern part and CO_2 coming from the south (Hässig et al. 2015), which may explain the large difference between the two hemispheres for the relative sulphur-bearing species abundances. In this paper, we extend the investigation of sulphur-bearing compounds to a much larger time interval which covers heliocentric distances from 3.5 to 1.24 au and which also covers the equinox early 2015 May, when the southern part became the summer hemisphere. Based on this extensive data set covering large heliocentric distances, it is possible to address the question of the bulk ice composition in 67P with respect to sulphur. During the more active part of the mission close to perihelion, additional sulphur-bearing species were detected which are also discussed.

2 OBSERVATIONS

In this paper, the distances between *Rosetta* and 67P are given with respect to the nucleus centre and time stamps are given in UTC.

2.1 *Rosetta*/ROSINA

Since early 2014 August, the European Space Agency spacecraft *Rosetta* has been accompanying the Jupiter-family comet 67P. Part of the scientific payload is the ROSINA, which consists of two complementary mass spectrometers and a pressure sensor. Here we will only introduce the Double Focusing Mass Spectrometer (DFMS). The main characteristics of DFMS are a high mass resolution of $m/\Delta m$= 3000 at 1 per cent peak height on mass-to-charge ratio 28 u/e and its dynamic range of 10^8 making it possible to measure minor species. Besides this, DFMS is designed in such a way that it covers a mass range from m/z = 12–140 u/e, has good energy focusing properties in order that $\Delta E/E$ is up to 1 per cent and a high mass dispersion in the focal plane making it possible to use a position-sensitive detector (Balsiger et al. 2007).

2.2 Measurements

ROSINA was almost continuously sampling the coma since the beginning of mission in 2014 August. Thus, the S-bearing species H_2S, SO, OCS, S_2, SO_2, CS_2 and atomic sulphur could be followed over a long period between the spacecraft arrival in 2014 August and perihelion in 2015 August. Since H_2S is the major sulphur species in the coma, its evolution has been followed during the entire period between beginning of mission to perihelion. For the remaining species listed before, data between equinox in 2015 May and perihelion in 2015 August have been analysed. Furthermore, our work has focused on several periods for which the local densities were high:

(i) October 2014, when *Rosetta* was within 10 km distance to the comet centre for about 15 d;
(ii) February 14 during a subsolar flyby going down to 8 km;
(iii) March 28 during a flyby going down to 15 km;
(iv) July 30–31 for SO and CH_3SH because 67P was almost at perihelion and *Rosetta* was closest to the comet within the following six weeks.

Those four periods were scrutinized for the presence of S-bearing molecules other than those listed above since the high local densities permit observations of minor species. Fig. 1 shows *Rosetta*'s orbital parameters such as the latitude in the frame attached to comet 67P (Scholten et al. 2015) and heliocentric distance between

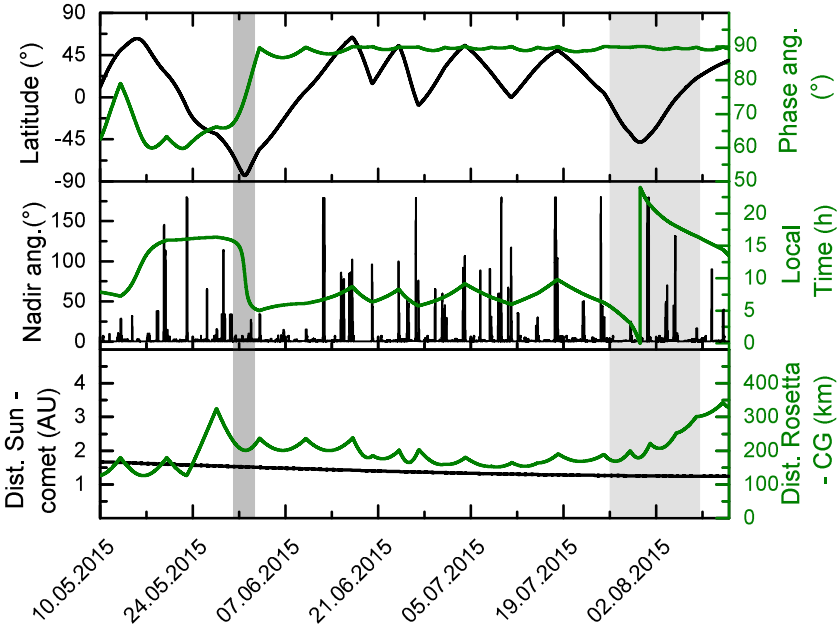

Figure 1. Orbital parameters' time series of *Rosetta* between equinox on 2015 May 10 and perihelion 2015 August 13. The upper panel shows the subsatellite latitude as defined by Scholten et al. (2015) and the phase angle. In the middle panel, the nadir-off pointing and local time are shown while the lower panel shows the heliocentric and the cometocentric distance. The first dark grey rectangle denotes the period as the phase angle changed from about 60° while the second light grey rectangle denotes the period when *Rosetta* did the transition from the equator to −45° back to the equator.

equinox May 10 and perihelion 2015 August 13. The uppermost panel shows the subsatellite latitude and the so-called phase angle which is defined as the angle between the Sun–comet line and the spacecraft–comet line, e.g. a phase angle smaller than 90° means *Rosetta* was in between Sun and 67P. For the phase angle, there is one significant change at the end of May. There the phase angle changes from 60° to 90° while *Rosetta* was over South Pole. This is indicated by the grey dark bar in the graph. Starting one month after equinox, *Rosetta* spent two months solely over northern latitudes. During this period, the subsolar point went from −13° to −40° , thus in the Southern hemisphere from spring to summer. The second grey bar indicates the period when *Rosetta* went from the equator to −45° and back to the equator while doing a transition from 200 to 300 km. The middle panel of Fig. 1 shows the nadir angle and the local time. Since DFMS is mounted on *Rosetta*'s instrument platform, deviation from nadir pointing is given by the spacecraft attitude. As can be seen from the middle panel, most of the time *Rosetta* pointed within ∼10° from nadir. Only between 2015 June and August roughly every two weeks a slew larger than 20° was performed. Since DFMS's field of view for neutral measurements is ±20° in general, the entire comet was covered while pointing nadir ± a few degrees. Consequently, no significant differences should be present due to nadir-off pointing for the data set between equinox and perihelion (except maybe for periods when the spacecraft was slewing). The local time does not take into account the comet's shape and thus the illumination conditions. The bottom panel shows the changes in heliocentric and cometocentric distance.

3 DFMS DATA TREATMENT

All data used in this study were acquired with ROSINA/DFMS in high-resolution mode (see Balsiger et al. 2007). In the following section, the operation principle of DFMS and the data reduction will be summarized. Both have been explained in more detail by Le Roy et al. (2015) and references therein.

3.1 DFMS operation principle

DFMS is operated in such a way that positively charged primary ions entering the instrument in neutral mode have energies outside the allowed energy range of $\Delta E/E = 1$ per cent. Thus, they will not be transmitted towards the detector. The ion source is located after the entrance slit. There neutral particles are ionized by electron impact ionization at 45 eV. This process leads to positively charged atomic and molecular ions, which are either the corresponding parent molecule or one of its fragments. Therefore, even in neutral mode, what is ultimately detected is/are the corresponding ion(s). In most cases, the ions are singly charged but occasionally also doubly charged particles are detected at half the mass. Due to its construction, DFMS can sample only a single mass spectrum in high-resolution mode at a time. In order to observe a certain mass-to-charge ratio (CM), a mass-dependent acceleration voltage is applied. Then the ions are guided towards the analyser which consists of a 90° electrostatic energy analyser and a 60° magnetic sector. In the electro static analyser, the ion beam is focused according to the ion energy while in the magnet focusing occurs based on the mass-to-charge value of the ions. The ions are detected by the microchannel plate/Linear Detector Array (MCP/LEDA), which consists of two MCPs in chevron configuration followed by a position-sensitive imaging detector (Berthelier et al. 2002; Nevejans et al. 2002; Balsiger et al. 2007). This detector consists of two rows (A and B) with 512 pixels each. Each impinging ion releases an electron cascade in the MCP depending on the ion's energy, species, the voltage applied on the MCP and its degree of deterioration. The incoming electron current on the LEDA is measured in analogue mode and converted to a digital signal. Before a spectrum is acquired, the on-board software sets the overall gain to one of 16 pre-defined gain steps (GS) which represent 16 different potentials applied on the MCP. Each spectrum represents 3000 individual 6.6 ms scans which are added together. For CM above 70 u/e, an additional potential is applied at the front plate of the MCP to enhance

the ion energy and consequently enhance the electron cascade in the MCP.

3.2 Data reduction

The nominal data reduction procedure for DFMS MCP-LEDA data is done in five steps: (i) subtract LEDA offset, (ii) convert Analog-to-Digital-Converter (ADC) counts to ions per spectra, (iii) derive mass scale, (iv) determine signal per spectra for species j and (v) calculate number density for species j. Due to the working principle of the LEDA, first a charge (in other words an offset) has to be applied on each pixel (Nevejans et al. 2002). This offset on the detector can be represented by a polynomial of third order degree with different parameters for rows A and B. In principle, the shape of the curve is preserved for each row but the level can vary by about 10 per cent. However, a deviation of this shape has been observed for CM which are a few integer u/e away from 18 u/e, 28 u/e and 44 u/e. This deviation indicates that there are disturbances to the offset due to the high signal of the very abundant species. Therefore, for every spectrum, a polynomial is done in areas where no peaks are detected. The ADC counts ($\mathrm{counts_{ADC}}$) per pixel are converted to ion counts per pixel and spectra $n_{\mathrm{Ion}}(p)$ using

$$n_{\mathrm{Ion}}(p) = \frac{\mathrm{counts_{ADC}}(p) \cdot c_{\mathrm{ADC}} \cdot c_{\mathrm{LEDA}}}{\mathrm{pg}(p, \mathrm{GS}) \cdot g_{\mathrm{MCP}}(\mathrm{GS}) \cdot e \cdot y}, \quad (1)$$

where $c_{\mathrm{LEDA}} = 4.2 \times 10^{-12}$ F is the LEDA capacitance, $c_{\mathrm{ADC}} = 2.5/(2^{12} - 1)$ V is the ADC conversion factor, e is the elementary charge and y is the yield of the MCP (Meier & Eberhardt 1993). For DFMS, the MCP yield is part of the measured sensitivity since one cannot separate ionization, transmission and detection yield for calibration measurements. Besides the constant conversion factors, there are two operation time-dependent factors. First, there is the overall gain of the MCP depending on the applied GS $g_{\mathrm{MCP}}(\mathrm{GS})$. The second one is the dimensionless pixel gain correction factor $\mathrm{pg}(p, \mathrm{GS})$, which represents the deterioration over time due to releasing electron avalanches in the MCP for each individual pixel and GS. Measurements to determine these factors are executed regularly over the course of the mission. For GS which are not measured, an empirical law is applied to calculate the missing ones. In order to take into account that the detector deterioration is a time-dependent process, a linear interpolation is used between two pixel gain campaigns. For this study, the contribution of spacecraft background has not been taken into account because for the sulphur-bearing species only H_2S was present marginally before the encounter (range of a few detector counts) and for H_2O, CO and CO_2, the cometary signal is a few orders of magnitude higher than the spacecraft background before encountering 67P. In addition, only row A has been taken into account, which should have no impact since only relative abundances are presented. For DFMS, the pixel on the LEDA is associated with a certain mass per charge ratio. The relation is

$$M(p) = M_0 \cdot \mathrm{e}^{(p-p_0)\cdot x/(D\cdot z)}, \quad (2)$$

where $M(p)$ is the mass per charge for pixel p, M_0 is the set mass per charge ratio CM, p_0 is the centre of the ion beam associated with M_0, $x = 25$ μm is the distance between two pixels, $D = 127\,000$ μm is the dispersion factor and z is the zoom factor which is 6.4 for the data shown in this paper. For a more detailed description, the authors refer to Le Roy et al. (2015).

An automatic analysis software has been used to determine the peak area, relative to number of detected ions, corresponding to S, H_2S, SO, S_2, OCS, SO_2, CS_2, H_2O, CO and CO_2. It uses a simplex algorithm, which yields consistent results. However, in order to obtain accurate results, the characteristics of DFMS and the available knowledge on the coma constituents of 67P are taken into account. This means the mass scale is defined based on the identified peaks in a spectrum. In the case of overlapping species, we use an analytical description of a single species signal, which can be described by the sum of a narrow high Gaussian and a broad small Gaussian, as introduced by Le Roy et al. (2015). Unfortunately, S_2 could only be determined using the software between the mission start and a few weeks after equinox. After these times, the signal became too low and data had to be analysed manually. For comparison between manual and automatic analysis, the entire data set from 2015 July has been selected, since higher signals close to perihelion were expected. Another special case is SO because there is an interference with CHCl. The automatic analysis software could not fit this properly since the peaks were too close together. Samples from each of the four periods yielded a deviation of the signal due to SO, and the maximum deviation between automatic and manual analysis is 20 per cent. In order to follow SO over the mission, the signals of both SO and CHCl have been used. For the CS, H_2CS, CH_3SH and C_2H_6S, the automatic analysis could not be used as there were too many interferences with other species or the signal-to-noise ratio was too low. These spectra have been analysed semi-automatically using a constrained least-squares fit. The constraints were obtained from the peak centre of the identified species. The number density of species j (n_j) in the vicinity of DFMS entrance is given by

$$n_j = \frac{n_{j,\mathrm{Ion}} \cdot \frac{e}{t_{\mathrm{int}}}}{\frac{Q_j}{\sum_i Q_i} \cdot S_j}, \quad (3)$$

where $n_{j,\mathrm{Ion}}$ is the number of ions in the spectra due to species j, $t_{\mathrm{int}} = 19.8$ s is the total integration time per spectra, $\frac{Q_j}{\sum_i Q_i}$ is the fragmentation of j relative to the total amount of fragments produced in DFMS's ion source and S_j is the total sensitivity of the species j. In order to obtain the correct value for $n_{j,\mathrm{Ion}}$, the measured signal has to be corrected for the contribution from other species. For example, S is produced through electron ionization of every sulphur-bearing species in the ion source of DFMS. Thus, the signal on m/z 32 u/e for S has to be corrected for all the contributions at 32 u/e originating from other S-bearing molecules. Due to the sequential nature of the DFMS measuring mode, different species are in general not obtained simultaneously. Therefore, for the purposes of corrections between species and comparison between species, the closest measurements within 40 min have always been used. If there was none, then the data set has not been taken into account. Species fragmentation patterns and sensitivities are instrument-specific. Consequently, calibration measurements need to be done with the instrument copy of DFMS in the lab. However, it is not possible to calibrate every species seen in the coma since some of them are dangerous for human health and/or the instrument like HCN, for example. For these species, the fragmentation pattern from the National Institute of Standards and Technology (NIST) data base (Stein et al. 2016) is used as a first approach. Both NIST and DFMS use the same process for ionization, but the electron energy used is different. For NIST it is 70 eV while the nominal value for DFMS is 45 eV. Laboratory work with DFMS has shown that in general slightly fewer fragments are produced in DFMS. Consequently, using NIST fragmentation patterns will lead to a slight underestimation of the parent molecule. For some molecules like H_2CS, there are no fragmentation patterns reported in the NIST data base. In such cases, the fragmentation pattern of a molecule with similar structure and constituting molecules has been used. For the sensitivity, an empirical relation between the

Table 2. Fragmentation pattern and sensitivity used to calculate relative abundances.

Species	Fragmentation pattern	Sensitivity
S	Estimated (based on isotopic ratios)	Calculated[a]
OCS	NIST[a]	Calculated[a]
S_2	NIST[a]	Calculated[a]
CS_2	NIST[a]	Calculated[a]
H_2CS[b]	NIST – CH_2O	Calculated[a]
CH_3SH	NIST[a]	Calculated[a]
C_2H_6S	NIST[a]	Calculated[a]
SO_2	NIST[a]	Calculated[a]
H_2O	Measured	Calculated[a]
CO	Measured	Calculated[a]
CO_2	Measured	Measured
H_2S_2[b]	NIST – C_2H_2	Calculated[c]
S_2H[b]	NIST – C_2H_2	Calculated[c]

[a]Same as used by Le Roy et al. (2015).
[b]No fragmentation pattern available in NIST data base.
[c]No electron impact ionization cross-section reported in the literature. The one of S_2 is used to derive the sensitivity.

CM of the parent molecule and the sensitivity has been established. The input parameters are the CM of the parent ion e.g. for CH_3SH it would be 48 u/e and the ionization cross-section at 45 eV that has been taken form the NIST data base (Llovet et al. 2014). Table 2 lists the detected species and references for their fragmentation patterns and sensitivities used to derive the reported number densities.

3.3 Measurement uncertainties

Part of the data reduction is the correction for the deterioration of the MCP and its gain over the course of the mission. In order to determine the deterioration, calibration measurements are done on a regular basis and the uncertainty due to these corrections is assumed to be not larger than 7 per cent. The remaining uncertainties are given by the uncertainty of the overall gain (5 per cent) and the uncertainties of measured sensitivities and fragmentation patterns. For species which were not calibrated with the instrument copy in the lab, the situation is more difficult since here we can only estimate the uncertainties introduced using NIST values and calculated sensitivities. We generally assume in this case a 10 per cent uncertainty for the fragmentation pattern. The uncertainty of the sensitivity can be up to a factor of 2. This represents a constant systematic uncertainty which affects absolute abundances and ratios while the relative change of these is not affected. As a consequence, this systematic uncertainty is not taken into account for the error propagation as it would mask the real changes in signal. However, this bias will be discussed together with the final results. For SO, another 20 per cent has been taken into account since at least 80 per cent of the peak area of the cumulative peak of SO and CHCl determined automatically is due to SO. Based on the uncertainties described above, we obtain the final statistical and methodical uncertainties for densities and relative abundances.

4 RESULTS

This section is divided into five subsections.

(i) First, we present the detection of S-bearing species never before observed in comets.

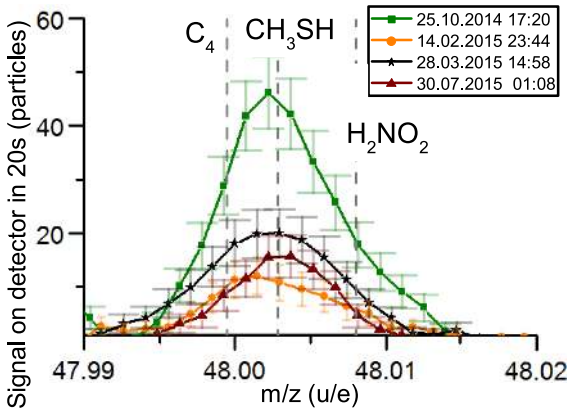

Figure 2. Mass spectra showing m/z 48 row A. For each of the selected periods, an example spectrum has been selected. Identified species are indicated by a dashed line.

(ii) Then we focus on the question whether S, SO, H_2CS and CS are of cometary origin or a product of fragmentation of higher mass parent species in DFMS's ion source.

(iii) Afterwards we show the quantitative impact of photodissociation and photoionization on the species in the coma.

(iv) For H_2S, the changes in abundance relative to H_2O are shown in order to see how the major species contribute to the S and O budget over the mission.

(v) For S, SO, OCS, S_2, SO_2 and CS_2, the changes in abundance relative to H_2S are presented between equinox in 2015 May and perihelion in 2015 August.

(vi) The evolution of the SO/SO_2 ratio is presented between equinox and perihelion.

(vii) Finally, the elemental abundance S/O based on the local densities of the above-mentioned species and H_2O, CO, CO_2 and O_2 between equinox and perihelion in 2015 August is presented.

4.1 Detection of new S-bearing species

4.1.1 Observation of CH_3SH *and* C_2H_6S

The equivalent of methanol with S substituting O is methanethiol (CH_3SH). In Fig. 2, for each of the selected periods, a sample spectrum is shown. From this graph, it can be seen that CH_3SH has an interference with C_4 and H_2NO_2. However, the latter one is of minor importance. The peak is too broad to be solely due to C_4, and of the C, H, N, O and S-bearing molecules CH_3SH fits best.

In 2014 October during the 10 km period, a signal on the m/z 62 u/e temporarily appeared which could be linked to C_2H_6S. In total, four spectra show this signal in 2015 October. In addition, it could be detected again during 2016 March 28 when local coma densities were comparable. From both periods, two representative spectra are shown in the right-hand panel of Fig. 3. It is seen that the peak is not centred on C_2H_6S, most likely due to the presence of C_5H_2, a fragment of a heavier hydrocarbon. The mass scale has been calibrated thanks to the presence of $OC^{34}S$ that is not shown here. The peak around m/z 62.015 u/e is slightly asymmetric indicating the presence of an additional species. A preliminary search suggested CH_4NO_2, but this will not be discussed further here.

As a consequence of the similarity in mass-to-charge ratio of C_2H_6S and C_5H_2, mass spectra at lower integer m/z ratio have to be checked for corresponding fragments of both molecules for the unambiguous detection of C_2H_6S. This is further complicated

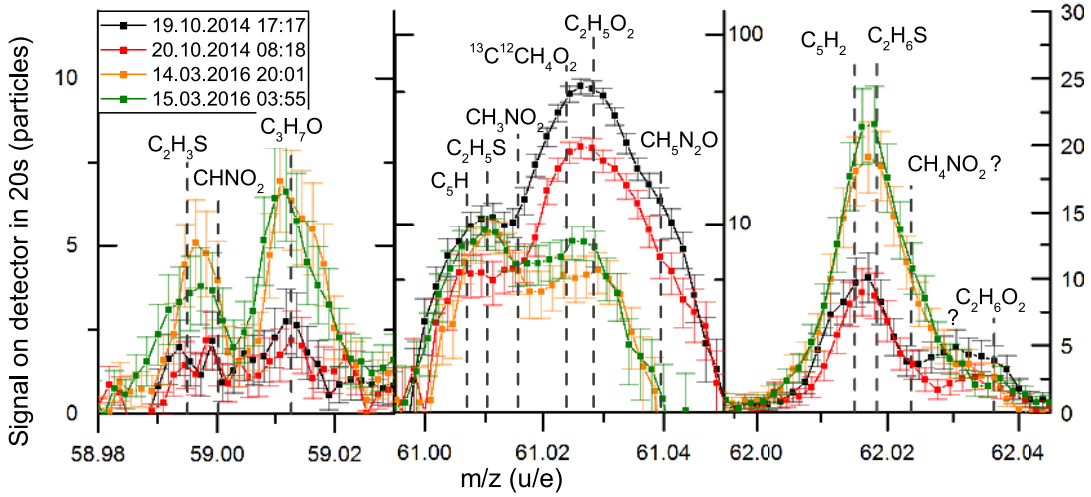

Figure 3. From right to left are shown mass spectra with m/z 59, 61 and 62 u/e of DFMS MCP-LEDA row B. Two of the measurements were acquired in 2014 October during the 10 km orbits and two around equinox in 2016 March. Identified peaks are indicated with labelled dashed lines.

because C_2H_6S has two isomers ethanethiol and dimethyl sulphide. The major difference in fragmentation pattern according to NIST is for the fragment CH_3S on m/z 48 u/e which is formed from ethanethiol and dimethyl sulphide by 47 per cent and 96 per cent of the parent, respectively. Unfortunately, CH_3SH contributes as well to CH_3S. The signal (not densities!) of CH_3SH is about an order of magnitude larger than that of C_2H_6S. Thus, nothing can be learned about the structure of C_2H_6S from the measured CH_3S. For most of the major fragments of the two isomers, there is interference with another species or its fragments. This leaves signals above m/z 59 u/e for comparison. The most abundant fragment with $m/z > 59$ u/e is on m/z 61 u/e but this mass there is the overlap with C_5H as can be seen from the middle panel of Fig. 3. In order to have no interference with the fragments of the type C_xH_y, one has to check m/z 59 u/e on which, according to NIST, a signal relative to parent between 3 per cent and 7 per cent is expected for ethanethiol and dimethyl sulphide, respectively. The corresponding mass spectra of 59 u/e are shown in the left-hand panel of Fig. 3. It can be seen that the signal appears rather small. In addition, there might be a contribution from CH_2NO_2, and by comparing the amplitude of the peaks on m/z 59 and 62 u/e, none of them fits with the fragmentation pattern of NIST. However, the presence of a signal on m/z 59, 61 and 62 u/e confirms that C_2H_6S is present in the volatile phase of 67P. Although it cannot be distinguished between the two isomers ethanethiol and dimethyl sulphide.

4.1.2 *Observation of* S_3 *and* S_4

Already at about 2 au it became evident that molecules with masses up to 100 u/e, at the end of DMFS nominal mass range, were present. In 2015 March during a close flyby, signals on *m/z* 96 u/e were detected in 14 spectra acquired over a period of 12 h. Careful data analysis indicated S_3 to be a likely candidate. When 67P was closer to perihelion and the environment became dusty, it became evident that molecules with higher masses were present as well. The m/z range was therefore increased up to 140 u/e. The higher the measured mass, the lower the sensitivity. Nevertheless, DFMS detected some molecules in this mass range. Among these were again clear peaks on *m/z* 96 u/e and in addition on 128 u/e. Careful data analysis revealed that these peaks are due to S_3 and S_4. It is not clear if these are real parent molecules or if they are the products

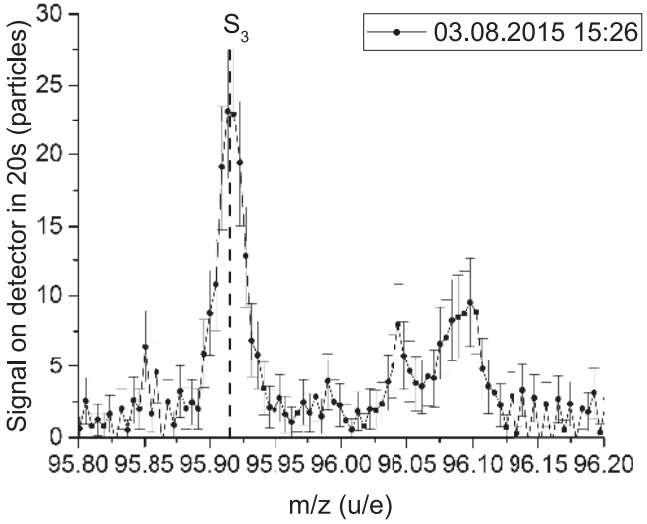

Figure 4. Mass spectrum of row B showing m/z 96 u/e acquired close to perihelion on 03.08.2015.

of even heavier S_n, which fragment into S_3 and S_4 Fig. 4 shows the spectra of the highest signal of S_3 acquired with row B. However, it is very likely that these species represent the products of radiolysis of H_2S ice as described in e.g. Woods et al. (2015). The condensation temperature of S_3 is ∼280 K. For S_4 it is even higher. It is unlikely that they desorb directly from the nucleus, as the surface temperature of the nucleus is too low even at perihelion according to the model of de Sanctis, Capria & Coradini (2005). Their model predicts surface temperatures on the dayside at perihelion to be below 260 K for a dusty crust and to be lower than 200 K for the water-containing layer underneath. Temperatures are therefore most likely not high enough to release S_3 or S_4 directly from the nucleus. Dust grains released into the coma can reach much higher temperatures (Lien 1990), thus making the release of S_3 and S_4 possible. There is circumstantial evidence pointing to dust as source. First of all, S_3 has been detected during the flyby in March where a considerable amount of dust was in the vicinity of *Rosetta* resulting in a safe mode of the spacecraft. Secondly, the further S_3 detections have all been done during a slew of *Rosetta* on 2015 August 4 when *Rosetta* turned its instrument platform more towards the Sun. In the foregoing

measurement period between the end of 2015 July and 2015 August 4, the instrument platform of *Rosetta* was hardly sunlit and *Rosetta* was in dusty environment as it approached perihelion. Thus, it is assumed that some dust grains were collected and preserved. During the slew on 2015 August 4, some of it is thought be exposed to the Sun, heat up and disintegrated. Thirdly, previous and subsequent slews of the same kind did not result in further detections of S_3 and S_4 indicating that the reservoir was depleted. Fourthly, the same measurement procedure during the cruise phase of *Rosetta* did not result in further detections; thus, it is unlikely that S_3 and S_4 were part of the spacecraft background.

There are only a few measurements of these species always associated with clear signatures of dust. As S_3 and S_4 are most likely embedded in dust, it does not make sense to give abundances relative to water. None the less, an estimation of the S_3/S_4, S_2/S_3 and S_3/H_2S ratios can be obtained. However, one has to be aware that these ratios are uncertain by large factors, even up to factors of 10. The reasons are as follows. First, it is unknown whether S_3 and S_4 are fragments of another molecule like S_8 and whether the fragmentation occurred in the instrument or by thermal degradation beforehand. In such a case, the S_3/S_4 ratio would be meaningless for the understanding of comets. Secondly, DFMS has not been calibrated for such species and there is no information about fragmentation pattern and ionization cross-section available in the literature so that the sensitivity of species like S_3...S_8 could be estimated. Thirdly, the source of S_3 and S_4 is most likely a (semi-)refractory compound, and it is likely that it accumulated during the weeks before the slew. Thus, it could be enhanced by an unknown factor compared to the volatile part of 67P or it could be depleted because only a certain fraction was collected or outgassing on/from *Rosetta*. Fourthly, there is only one measurement of S_3 and S_4, and due to DFMS's measurement principle the period in between is 24 min. No estimation on how this affects the measured S_3/S_4 ratio can be given. And to compare to S_2 and H_2S is even worse. There the time between two measurements is about 1 and 2 h, respectively. A direct comparison of the measured ion current yields for $S_3/S_4 \approx 3$, for $S_3/S_2 \approx 3$ and for $S_3/H_2S \approx 0.01$. As elaborated in the foregoing paragraph, these values have large uncertainties.

4.1.3 Search for H_2S_2 and S_2H

Laboratory experiments of UV irradiation of ice mixtures of H_2S and H_2O lead to the formation of S_2H and H_2S_2 in the ice (Jiménez-Escobar et al. 2012). To check the presence of these molecules in the coma of 67P, October 25 has been selected because during the 10 km orbits the local density for H_2S on this day was very high. In Fig. 5, we show four representative spectra of m/z 65 u/e, acquired between 23.10.2014 12:00 and 26.10.2014 02:20 which is equivalent to more than one full rotation of 67P, together with identified species indicated by dashed lines. Fig. 5 shows no distinct peak due to S_2H, which is further complicated by the interference between S_2H and $^{33}SO_2$. It is not possible to check for the presence of H_2S_2 since it has almost the same mass-to-charge ratio as $^{34}SO_2$ and cannot be resolved by DFMS.

4.2 Origin of S, SO, H_2CS and CS

4.2.1 Atomic sulphur

The ROSINA measurements show a surprisingly large amount of atomic sulphur (S) in the coma of 67P. In order to determine the

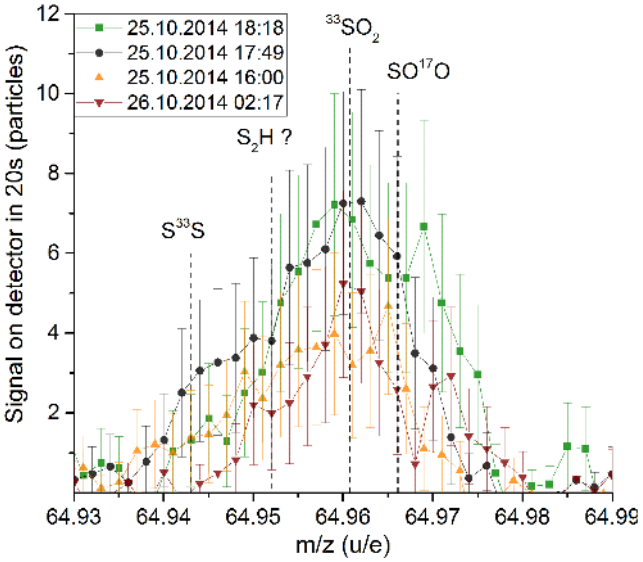

Figure 5. Representative spectra of m/z 65 u/e during 10 km orbits in 2014 October.

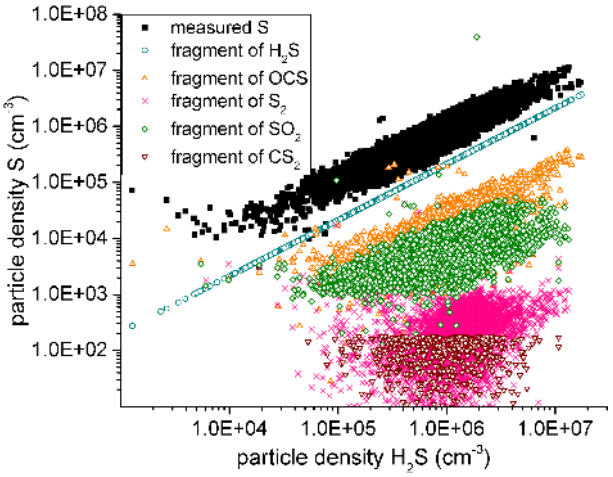

Figure 6. Number density of measured S and the contribution from S-bearing molecules to it, with respect to H_2S.

amount of atomic sulphur, one has to take into account the contributions from the heavier S-bearing molecules. These contributions arise from electron ionization of S-bearing molecules into $S^+ + A$ inside the mass spectrometer whereas A can be $[X] + e^-$, $[X]^-$ or $[X]^+ + 2e^-$. After the subtraction of all these contributions, the remaining S-signal is due to atomic sulphur in the coma. Fig. 6 shows an overview of these contributions, for the major S-bearing molecules using the data since beginning of the mission until 2015 August. One can see a strong correlation between the measured atomic sulphur signal and H_2S, which is the most dominant source of fragmented sulphur. Good knowledge of the molecules' individual fragmentation patterns is essential to make accurate statements about the different contributions and finally the amount of atomic S. DFMS was calibrated for H_2S, but for other compounds the NIST data base was used (see Table 2). On average, the ratio between S due to H_2S and total measured S is about 20 per cent while all the other contributing molecules together deliver about 5 per cent of the total measured S. To explain the total measured S with H_2S in the coma, one would need about a factor of 5 more H_2S than

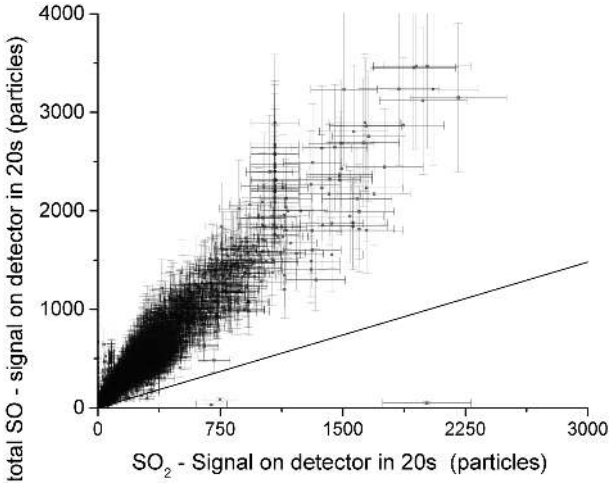

Figure 7. Total measured SO abundance including contribution from fragmentation of SO_2 (black squares). The black line shows the contribution to SO by fragmentation of SO_2 inside DFMS's ion source.

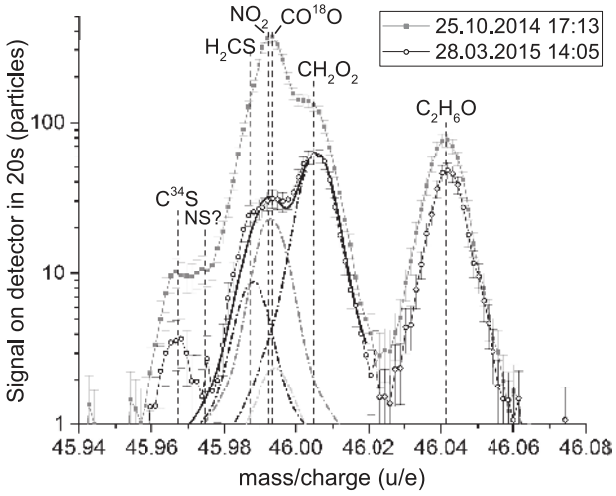

Figure 8. Mass spectra of m/z 46 u/e (row A). Identified species are indicated by dashed lines. In black is shown the signal during the flyby on 2015 March 28 when the signal of CO_2 was comparably low while in grey the typical signal on m/z 46 u/e is shown. For the measurement of March 28, the fit is shown with dash–dotted lines while the cumulative fit is drawn in black.

detected. All other sulphur-bearing species, even with larger uncertainties in terms of DFMS's fragmentation pattern, cannot account for the signal on atomic sulphur. Thus, atomic sulphur can be clearly identified as a species in the coma though its origin, whether it is released from a substance on the surface or within the nucleus, is not clear yet.

4.2.2 SO

First, it has to be asserted whether SO is indeed released from the nucleus. This is important as SO also forms through photodissociation in the coma and, more importantly, through electron impact ionization of SO_2 inside the ion source of DFMS. According to NIST, 49 per cent of SO_2 fragments into SO^+ ions by electron impact bombardment, the type of ionization used in DFMS. Therefore, based on the abundance of SO_2, a corresponding amount of SO has to be subtracted from the total SO signal. Fig. 7 shows the measured total signal of SO with respect to SO_2 between beginning of the mission in 2014 August and perihelion. The black line indicates the amount of SO expected from dissociation of SO_2 in DFMS in case the comet contains no parent SO. Theoretically, no signal for SO can be below (the black line) what is produced by the fragmentation of SO_2 inside the instrument. However, given that DFMS measures SO and SO_2 not at the same time but with a time shift of approximately 8 min, the SO abundance can occasionally drop below this line, even more so when the spacecraft attitude changes within the observation period. Nevertheless, it becomes apparent that SO_2 alone cannot explain the observed signal of SO. OCS (carbonyl sulphide) is the only other species detected so far containing S and O. But according to NIST, its fragmentation does not produce SO ions. According to Huebner & Mukherjee (2015), the photodissociation rate for SO_2 to SO is at 1 au $1.59 \times 10^{-4} s^{-1}$. As a consequence, the contribution to SO is negligible as the gas propagation time is merely seconds from the surface of the comet to *Rosetta* (see Table A1). Sulphur monoxide can therefore clearly be identified as a species in the coma, i.e. to be present in the ices in the form of SO, outgassing from the nucleus itself and/or from an additional source.

4.2.3 H_2CS

The signal of thioformaldehyde (H_2CS), the equivalent of formaldehyde, has a mass-to-charge ratio of about 46 u/e. Unfortunately, $C^{16}O^{18}O$ has a similar mass-to-charge ratio. Therefore, the signal of H_2CS, if present, is most of the time hidden in the signal due to the isotopologue of CO_2. Nevertheless, during the close flyby on 2015 March 28, the density of CO_2 was low enough to reveal the corresponding signal of H_2CS. In Fig. 8, we show the typical signal of the *m/z* 46 u/e in grey (squares), the spectra with the least contribution of $C^{16}O^{18}O$ during the flyby in black (circle) and the fit considering H_2CS, NO_2 and $C^{16}O^{18}O$. Indicated by dashed black lines are the location of identified species as $C^{34}S$ or C_2H_6O. Although there is no distinct peak due to H_2CS, there is as well not a distinct peak due to $C^{16}O^{18}O$ and NO_2 as in other cases. This signal shape is best explained by two or more species with similar signal strength close to each other. Of all species with a lower mass-to-charge ratio than NO_2, it is H_2CS which fits best. However, the signal has to be corrected for the fragment of CH_3SH which was present as well. In Fig. 9, a comparison is done between the measured signal (not density) of H_2CS and the fragment of CH_3SH. The first two and the last measurements of H_2CS could be explained solely by the presence of CH_3SH taking into account uncertainties (σ). However, this is not the case for the remaining measurements. Even assuming 3σ boundaries, H_2CS could only be explained in half of the remaining cases by fragmentation of CH_3SH inside DFMS. In addition, no distinct signal due to C_2H_6S. Consequently, thioformaldehyde can be clearly identified as a species in the coma, i.e. to be present in the ices in the form of H_2CS, either outgassing from the nucleus itself or from an additional source.

In addition to H_2CS, the spectrum of 2014 October 25 at 17:13 UTC indicates the presence of an additional species because the signal does not decrease between $C^{34}S$ and the cumulative peak of $C^{16}O^{18}O$, NO_2 and H_2CS (Fig. 8). Considering volatile species bearing C, N, H, O and S, it is NS which fits best. However, a first check of the 10 km data in 2014 October for other and stronger signals at the location of NS was not successful. This is therefore only a tentative detection.

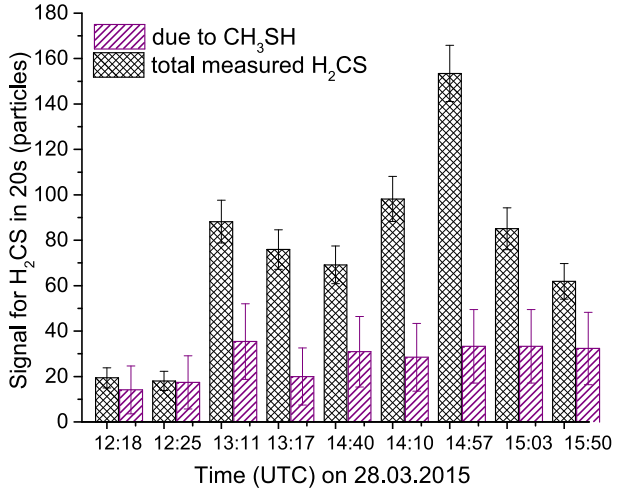

Figure 9. H_2CS budget during flyby in 2015 March (1σ). For each contribution, 1σ error bars are given.

4.2.4 CS

The radical CS has been detected in numerous comets by remote sensing observations (see Table 3) but for 67P no CS has been reported yet. In terms of DFMS, it has an interference with CO_2 on m/z 44 u/e. Thus, similar to H_2CS, the best chance to detect CS is when CO_2 is comparably low. In addition, it is crucial to know how much CS is present due to the fragmentation of H_2CS, OCS, CS_2 and CH_3SH. The contribution due to C_2H_6S can be neglected first because the parent signal is already small and second according to NIST only about 4 per cent of the parent fragments into CS. The analysis is then restricted to the flyby during 2015 March when H_2CS was detected. In Fig. 10, the total measured signal of CS is shown in grey. In addition, the contributions to CS from other molecules are shown. The largest contribution to CS, produced inside DFMS, is due to OCS followed by CS_2, H_2CS and CH_3SH. The total measured CS with 2σ boundaries lies within the calculated range (2σ) of CS fragments. Thus, CS was not detected in the coma of 67P in 2015 March. Thus, contrary to SO and S, CS is not originating directly from the nucleus of 67P. Outside of this period, no statement can be done since a possible CS signal was in general overlapped by the signal of CO_2.

4.3 Abundance ratios

4.3.1 Impact of photodissociation and ionization on abundance ratios

Most of the time between equinox and perihelion *Rosetta* spent within 200 km of the nucleus while the heliocentric distance was decreasing from 1.66 to 1.24 au. Closer to the Sun, photodissociation and ionization potentially become more important for the coma composition since the rates increase. Photodissociation and ionization rates for most sulphur-bearing species in this study have been computed from the values by Huebner & Mukherjee (2015) at 1 au for active and quiet Sun. Here we used the values for quiet Sun. The photodissociation and ionization rates at different heliocentric distances have been estimated assuming a $1/r^2$ law. In order to take into account the distance to the comet, it has been assumed that $N = N_0 \cdot \exp^{-\beta \cdot t}$, where β is the photodissociation/ionization rate at a certain heliocentric distance and t the time it takes for a particle to fly from the nucleus' surface to the spacecraft. Based on the

Table 3. Assumed bulk values ($\pm\sigma_{mean}$) in the coma of 67P relative to H_2O and H_2S, respectively. The upper panel gives the ratio without taking into account loss and gain of species in the coma due to photodissociation/ionization while in the lower panel the values have been corrected (see Section 4.3.1).

Relative to	H_2S	S^a	SO^b	OCS^c	$S_2{}^{c,d}$	$SO_2{}^c$	$CS_2{}^c$
Measured abundances							
H_2O	$(1.06 \pm 0.05) \times 10^{-2}$	$(4.81 \pm 2.84) \times 10^{-3}$	$(7.06 \pm 0.17) \times 10^{-4}$	$(4.04 \pm 0.09) \times 10^{-4}$	$(1.30 \pm 0.23) \times 10^{-5}$	$(1.24 \pm 0.03) \times 10^{-3}$	$(4.10 \pm 0.13) \times 10^{-5}$
σ	0.68×10^{-2}	0.21×10^{-3}	2.22×10^{-4}	1.18×10^{-4}	3.10×10^{-5}	0.45×10^{-4}	1.80×10^{-5}
H_2S (per cent)	100	50.7 ± 1.1	7.06 ± 0.17	4.43 ± 0.16	0.17 ± 0.03	12.68 ± 0.33	0.46 ± 0.02
σ (per cent)	–	14.4	2.22	2.06	0.32	4.31	0.13
Measured abundances corrected for photodissociation and ionization							
H_2O	$(1.10 \pm 0.05) \times 10^{-2}$	$(4.58 \pm 2.84) \times 10^{-3}$	$(7.1 \pm 1.1) \times 10^{-4}$	$(4.08 \pm 0.09) \times 10^{-4}$	$(1.97 \pm 0.35) \times 10^{-5}$	$(1.27 \pm 0.03) \times 10^{-3}$	$(5.68 \pm 0.18) \times 10^{-5}$
σ	0.68×10^{-2}	0.21×10^{-3}	2.3×10^{-4}	1.19×10^{-4}	4.69×10^{-5}	0.46×10^{-4}	2.49×10^{-5}
H_2S (per cent)	100	45.8 ± 1.0	7.06 ± 0.17	4.43 ± 0.15	0.25 ± 0.05	12.5 ± 0.3	0.61 ± 0.03
σ (per cent)	–	13.9	2.22	2.01	0.46	4.3	0.33

[a]Systematic uncertainty of sensitivity is estimated to be 50 per cent and not included here.
[b]Uncertainty of 20 per cent due to the automatic treatment is taken into account here.
[c]The systematic uncertainty of up to 200 per cent for the calculated sensitivity has not been taken into account here (for more details see Section 3.3).
[d]01.07.2015–26.07.2015 above positive latitudes and corrected for photodissociation/ionization: $S_2/H_2O = (2.93 \pm 0.46) \times 10^{-4}$, $\sigma = 6.35 \times 10^{-4}$, $S_2/H_2S = (3.41 \pm 0.35)$ per cent, $\sigma = 4.90$ per cent.

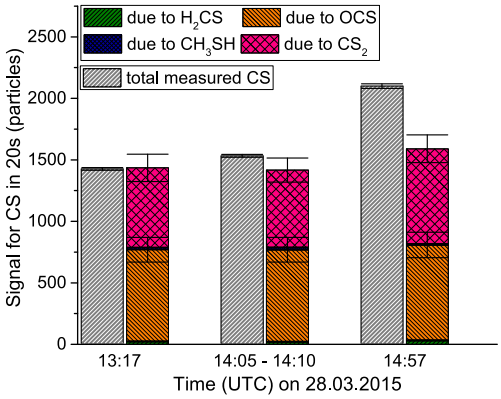

Figure 10. CS budget around the closest approach of the flyby in 2015 March. For each contribution, 1σ error bars are given.

presented velocity results for water by Gulkis et al. (2015), the outflow velocity has been assumed to be 700 m s^{-1}. The biases of a species due to photodissociation/ionization products have been taken into account, e.g. the measured SO signal has been corrected for the contribution of OCS and SO_2 and the loss of SO. Since *Rosetta* was most of the time within 200 km of the comet, we will discuss only this case here while in Table A1 the fractions of initial amounts at 200 and 300 km are given. Around equinox less than 5 per cent of H_2O, H_2S, S, OCS and SO_2 is lost due to photodissociation and ionization while for SO, CH_3SH and CS_2 it is 6 per cent, 24 per cent and 28 per cent, respectively. At perihelion, the fraction of dissociated H_2O, S, OCS and SO_2 is still smaller than 5 per cent while for H_2S, SO, CH_3SH and CS_2 it is 6 per cent, 11 per cent, 41 per cent and 47 per cent, respectively. For S_2 no photodissociation rate has been reported so far but De Almeida & Singh (1986) calculated a lifetime for S_2 of 250 s at 1 au for $\lambda \sim 280$ nm, which is very short. The loss has been estimated based on this number at equinox to be 34 per cent while at perihelion it is 52 per cent.

4.3.2 *Abundance of* H_2S *relative to water*

Fig. 11 shows the relative H_2S abundance compared to water. The spread of the values is considerable, ranging from below 0.1 per cent to almost 10 per cent. This is not due to uncertainties of the measurement as the statistical error is rather small, but rather to the relative position of the spacecraft to the comet, illumination conditions, seasonal and diurnal variations, and heliocentric distance.

H_2S is more volatile than H_2O. Whereas the sublimation temperature of H_2S is ∼80 K (Collings et al. 2004), a temperature which is reached according to de Sanctis et al. (2005) even at aphelion, the sublimation temperature for water is only reached inside of 3 au. One would therefore expect that the H_2S/H_2O ratio would drop dramatically with decreasing heliocentric distance outside of the water snow line, which is outside of ∼2.8 au. This is clearly not the case. In the beginning of the mission between 2014 August and November, which is heliocentric distances between 3.6 and 3 au, the ratio increased by a factor of 10. The spacecraft spent most of this time in terminator orbit sampling both hemispheres. There is a strong asymmetry between the two hemispheres where H_2S is depleted in the southern winter hemisphere (Fig. 12) early in the mission, thus following water and not CO_2 (Hässig et al. 2015), although H_2S is more volatile than CO_2. The Northern hemisphere at these large heliocentric distances is depleted in most volatiles (Le Roy et al. 2015). There are several possibilities why the ratio of water to more volatile species is different from the northern part of the neck. It could be due to layering as more volatile species have been sublimated whereas water has not. However, this is in contradiction to the fact that in the Southern hemisphere during the long winter this apparently did not happen, although temperatures according to de Sanctis et al. (2005) would have been high enough for the more volatile species. Then the Visible and Infrared Thermal Imaging Spectrometer has seen a recondensation of water from the interior (De Sanctis et al. 2015). However, this is a diurnal variation and would not explain our measurements which are seasonal and not diurnal, e.g. Rubin et al. (2014). As the excessive water production comes mainly from the neck area (Fougere et al. 2016) where there is a gravitational potential well, another explanation could be

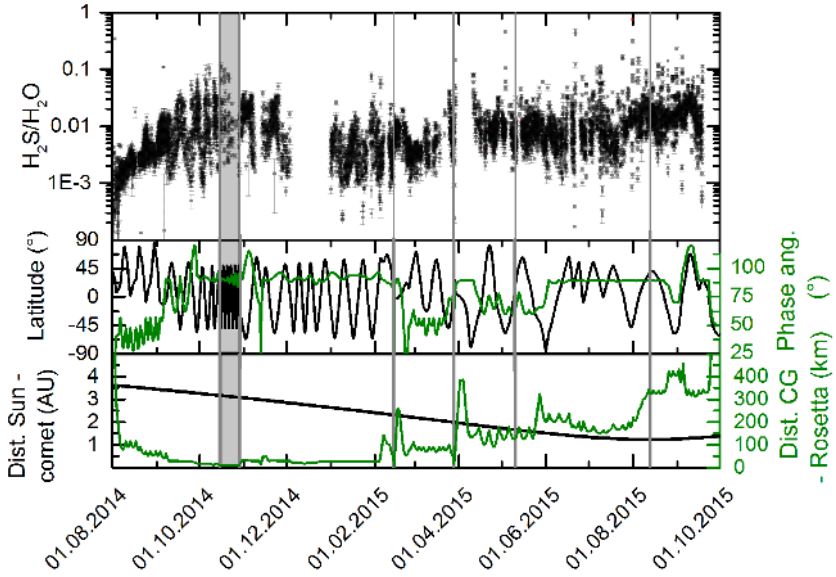

Figure 11. The uppermost panel shows the time series of H_2S relative to H_2O from beginning of mission in 2014 August till past perihelion one year later. Indicated by a grey area is the 10 km period in 2014 October, while the two flybys, equinox and perihelion, are indicated with solid grey lines. The middle panel shows subsolar latitude and phase angle while in the bottom panel the evolution of heliocentric and cometocentric distance is displayed.

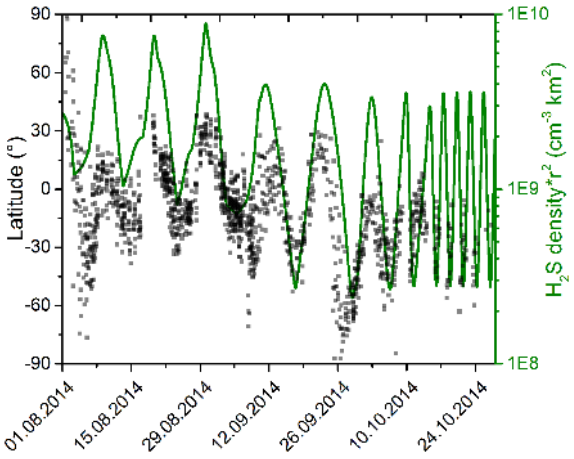

Figure 12. H_2S density multiplied by distance to comet squared for the period August 1 to the end of 2014 October together with the sub-spacecraft latitude. Statistical errors are smaller than symbol size.

transport of water ice grains during the perihelion passage to the dark side of the nucleus as observed earlier in the mission by the camera OSIRIS (Thomas et al. 2015). Like this the local ice composition would be changed in favour of water and in consequence it would appear to be less rich in volatiles.

Between 2015 February and end of June, the H_2S/H_2O ratio stayed remarkably constant. The sublimation temperature of pure H_2S ice in ultrahigh vacuum is 80 K (Collings et al. 2004). However, if H_2S is in a water matrix, a large fraction of the H_2S co-desorbs with H_2O in the 130–170 K temperature range, showing two maxima around 145 and 163 K (Jiménez-Escobar & Muñoz Caro 2011).

According to Jiménez-Escobar & Muñoz Caro (2011) and Viti et al. (2004), no sulphur-bearing species shows a desorption behaviour like CO in an ice matrix, although for example pure S_2 has a condensation temperature of 20 K, therefore even below CO. They classify the sulphur-bearing species according to their sublimation behaviour:

(i) HS, H_2S_2, OCS, H_2S, SO_2, HCS, NS as intermediate, showing two peaks when warmed up;
(ii) H_2CS, SO as water-like;
(iii) S_2, CS_2, S-residue as refractory.

The constant ratio between water and H_2S over many months and the strong very similar heterogeneity of the two species in the coma could very well reflect this desorbing pattern. From the end of June until perihelion in mid-August, the spacecraft encountered significant dust. The H_2S/H_2O ratio increased by at least a factor of 3. From this, we deduce that at least part of the H_2S is associated with dust grains or that deeper layers of the comet experienced temperatures above 82 K, the sublimation temperature of pure H_2S ice into ultrahigh vacuum (Collings et al. 2004). As cometary dust gets hot in the coma (Lien 1990), much hotter than the cometary surface, dust can shed its semi-volatile mantle, thus releasing many of the molecules which are most probably present in the dust mantle. Icy grains in the coma, which would mostly release water vapour, would not increase the H_2S/H_2O ratio. In addition, due to higher production rates and thus higher gas drag, there are also more and bigger dust particles in the coma, which are not only due to the surface layer of the comet, but are released by the jet-like features of the comet from the interior. The increase of H_2S/H_2O during perihelion is most probably not a purely seasonal effect as the spacecraft spent most of this time over the Northern winter hemisphere.

It is hard to say which value represents best the bulk H_2S/H_2O ratio for the comet. The most plausible value for the bulk is the value after equinox up to the start of the phase where there was significant dust. During this time, the less dust covered Southern hemisphere was sunlit and the comet was well inside the water ice line with sublimation of water and H_2S. The mean value corrected for photodissociation and ionization of H_2S/H_2O between 10.05.2015 and 30.05.2015 is (1.10 ± 0.05) per cent with $\sigma = 0.68$ per cent. The same period is used for all species to determine the bulk abundance.

4.3.3 Abundance of S, SO, OCS, S_2, SO_2 *and* CS_2 *relative to* H_2S *between equinox and perihelion*

Fig. 13 shows from top to bottom the abundance of S, SO, OCS, S_2, SO_2 and CS_2 relative to H_2S for the period between equinox and perihelion while the bottom panel shows the evolution of H_2S/H_2O. During this period, two significant changes in spacecraft attitude occurred. First, at the end of May 2015 *Rosetta* did a transition (highlighted in grey in Fig. 13) in phase angle from around 60° to 90° while going to the South Pole. Secondly, *Rosetta* went at the end of July after ∼6 weeks above the Northern hemisphere to 45° south (highlighted in light grey in Fig. 13) then back to the equator together with a transition from 200 to 350 km distance to 67P (for more details, see Fig. 1).

This separates the presented data into four parts which are discussed in the following.

During the first period between equinox and end of 2015 May, S, SO, OCS, S_2, SO_2 and CS_2 follow H_2S which itself follows water. Thus, these species follow water very closely at that time. As previously mentioned, we use this period when being above southern latitudes to estimate bulk abundances of the volatile species in 67P. With mean ratio to water of 0.011, H_2S is the most abundant S-bearing species in the coma of 67P. The second most abundant species is S with 45.8 per cent with respect to H_2S while SO_2, SO and OCS are in the 10 per cent range relative to H_2S. S_2 and CS_2 have a mean value relative to H_2S of less than 1 per cent and are thus trace species. The measured mean values and the ones corrected for photodissociation are given in Table 3.

Between June 2 and July 26, *Rosetta* was constantly above Northern hemisphere; nevertheless, the density of S_2 increased by a factor of ∼13 higher than the bulk value. The mean value for S_2/H_2S between July 1 and July 26 yields (3.41 ± 0.35, $\sigma = 4.90$) per cent. Then the subsolar point was between −26° and −40°; thus, in the Northern hemisphere there was winter. The significant increase between May (bulk) and July for S_2/H_2S implies that an additional source than sublimation from the nucleus is present for S_2 since the Northern hemisphere got less active. The fact that during the same period more dust was released implies a relation between the enhanced S_2 density and dust activity. In general, all species show more scattering between June 2 and 26. Nevertheless, they follow at large H_2S.

When *Rosetta* returned to the Southern hemisphere going down to −45° latitude for SO_2/H_2S and SO/H_2S, a distinct decrease is present. For the remaining S-bearing species, only the S/H_2S ratio might show the same qualitative behaviour. However, the size of scattering is too large to make a meaningful statement. For both periods highlighted in grey, *Rosetta* was measuring above the Southern hemisphere; nevertheless, the abundances relative to H_2S do not show the same behaviour. This might be explained by the location of the subsolar latitude. Around 2015 June 1, it was around −9° while beginning of 2015 August it was around −43°. Thus, in the

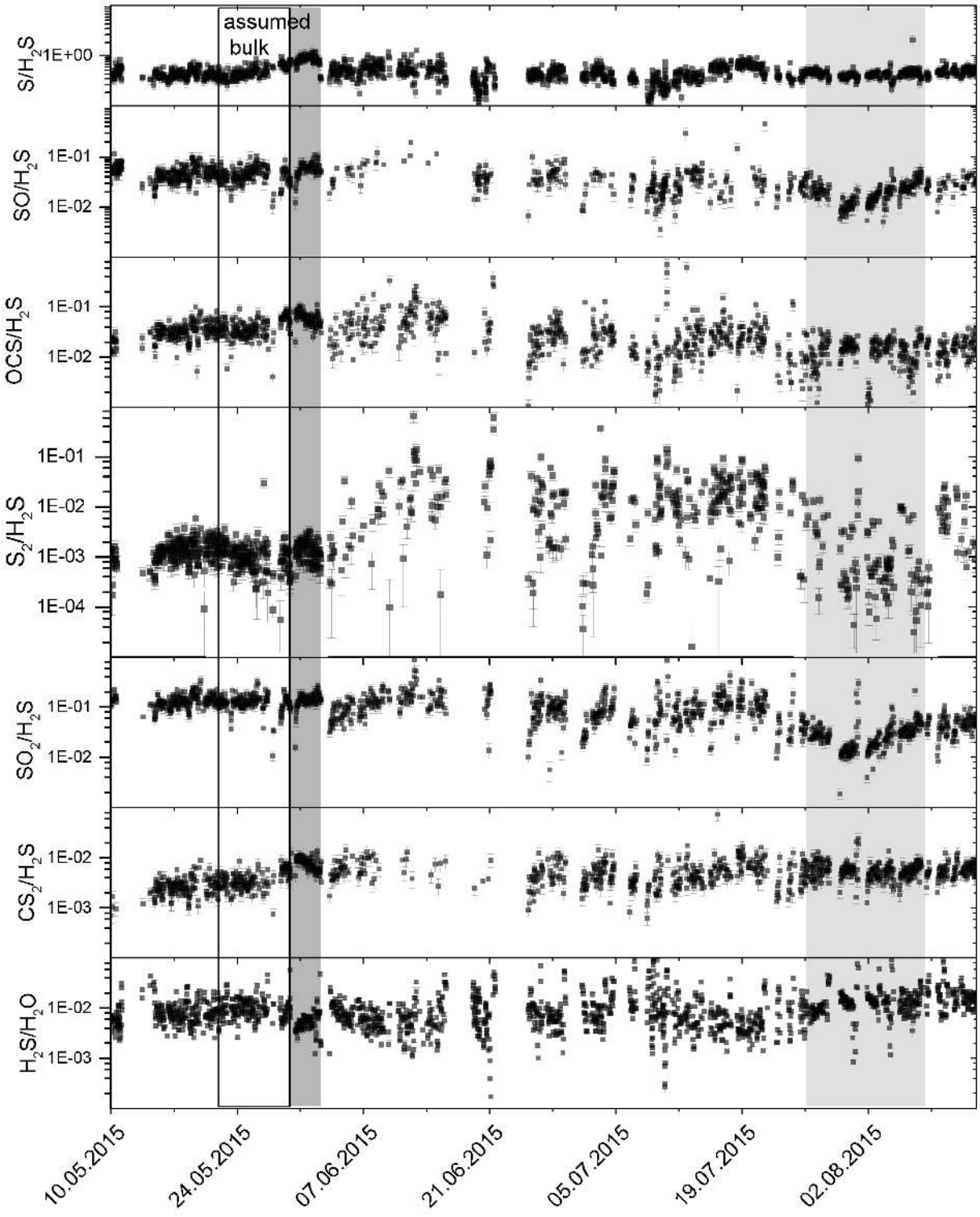

Figure 13. The first six panels going from top to bottom show the abundance of S, SO, OCS, S_2, SO_2 and CS_2 relative to H_2S, while the last one shows the corresponding H_2S/H_2O ratio. The shown data cover the period between equinox on 2015 May 10 and perihelion 2015 August 13. The first grey strip shows the transition of the phase angle from 60° to 90° while the second one in lighter grey shows the period during which *Rosetta* was going from 0° to −45° and back to the equator while doing the transition from 200 to 300 km.

first case, the Southern hemisphere was not yet in summer while in the latter one it was.

In essence, it is seen that none of the discussed species follow entirely H_2O nor H_2S. However, comparing the entire bulk period, the first two weeks of June and the period between July 26 and August 8, it can be seen that at least S follows more or less H_2S. This suggests in general a common origin in the ice matrix. In addition, OCS and SO_2 show the same general behaviour relative to

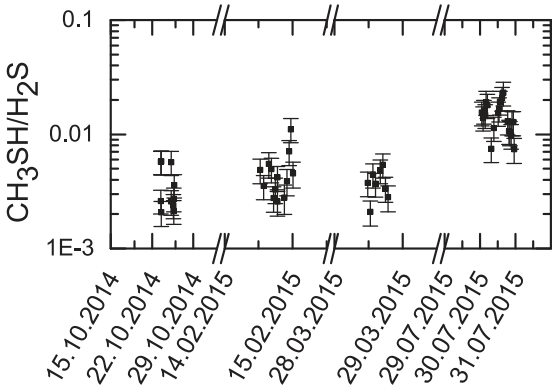

Figure 14. Relative abundance of CH_3SH to H_2S during the four selected periods without taking into account the effects of photodissociation and ionization.

H_2S. Both stay constant until mid-June, and then at the end of July they show a similar decrease. S_2 and CS_2 both show an increase comparing beginning of July with May. However, beginning of August while *Rosetta* was going to larger cometocentric distances only S_2 decreases but not CS_2. The decrease for S_2 is thought to be at least partly due to photodissociation/ionization, although the degree of decrease is a factor of 3 higher than what would be expected from photodissociation/ionization. It is not understood yet why CS_2 did not decrease but a plausible explanation could be an additional source.

Comparing the resulting bulk values corrected for photodissociation and ionization (lower panel Table 3) with the values reported by Le Roy et al. (2015), it becomes clear that the bulk abundances for OCS and CS_2 are somewhere between the Northern and Southern hemisphere values while for SO, SO_2 and S_2 the bulk is higher.

4.3.4 *Relative abundances of the organo-sulphur species to* H_2S

In the following paragraph, we present the abundances of all sulphur-bearing species relative to H_2S for which we do not have continuous data over the mission. For CH_3SH the ratio relative to H_2S is shown in Fig. 14 for the four selected periods. As one can see from Fig. 14 mean ratio of CH_3SH to H_2S is within errors the same during the end of 2014 October and during the two flybys in 2015 February and March, respectively. However, at the end of 2015 July it increased significantly to (1.44 ± 0.42) per cent. Applying the correction due to photodissociation of CH_3SH for the last period, the mean yields (3.5 ± 1.0) per cent relative to H_2S. The measured mean values with 1σ for the above discussed periods are given in Table 4.

Based on the measurements during the flyby on March 28 for H_2CS, a mean value of $(2.28 \pm 1.38) \times 10^{-3}$ for the abundance relative to H_2S could be determined. This value does not need to be corrected for photodissociation/ionization since measurements were obtained within 50 km distance to 67P at heliocentric distance of about 2.3 au. However, there is still the systematic uncertainty up to a factor of 2 which is not taken into account (see Section 3.3). Single values and the mean with 1σ are given in Table 5.

Table 4. Mean values ($\pm\,\sigma$) of CH_3SH relative to H_2S and H_2O, respectively. Systemic uncertainty of up to a factor of 2 (see Section 3.3) and the effect of photodissociation/ionization are not taken into account here.

Period	CH_3SH/H_2S (per cent)	CH_3SH/H_2O
2014 October	0.35 ± 0.12	$(2.85 \pm 1.11) \times 10^{-5}$
Flyby 14.02.2015	0.47 ± 0.22	$(4.98 \pm 3.80) \times 10^{-5}$
Flyby 28.03.2015	0.40 ± 0.08	$(2.64 \pm 0.64) \times 10^{-5}$
2015 July 30–31	1.44 ± 0.42	$(2.19 \pm 0.72) \times 10^{-4}$

Table 5. Relative abundances of H_2CS during the flyby in 2015 February with respect to H_2S and H_2O, respectively. At the bottom, the mean value ($\pm\,1\sigma$) is given. Systemic uncertainty of up to a factor of 2 (see Section 3.3) is not taken into account.

Time (UTC)	H_2CS/H_2S	H_2CS/H_2O
28.03.2015 12:14	$(5.27 \pm 1.45) \times 10^{-4}$	$(2.67 \pm 0.75) \times 10^{-6}$
28.03.2015 12:20	$(2.46 \pm 0.59) \times 10^{-3}$	$(1.30 \pm 0.32) \times 10^{-5}$
28.03.2015 13:07	$(1.78 \pm 0.43) \times 10^{-3}$	$(1.14 \pm 0.28) \times 10^{-5}$
28.03.2015 13:13	$(4.73 \pm 1.11) \times 10^{-3}$	$(3.21 \pm 0.78) \times 10^{-5}$
28.03.2015 14:00	$(1.92 \pm 0.47) \times 10^{-3}$	$(1.25 \pm 0.31) \times 10^{-5}$
Mean $\pm\,\sigma$	$(2.28 \pm 1.38) \times 10^{-3}$	$(1.43 \pm 0.97) \times 10^{-5}$

In the data of the 10 km orbits around 67P in 2014 October, a signal due to C_2H_6S could be identified in four spectra. Its presence could be confirmed by measurements from 2016 March when *Rosetta* was within 14–17 km distance to the centre of the nucleus. Thus, we had comparable local densities as in 2014 October. Assuming that the measured signal is either due to ethanethiol or dimethyl sulphide, the relative abundance to H_2S and H_2O could be derived for the four measurements (see Table 6). The resulting mean value with respect to H_2S assuming ethanethiol and dimethyl sulphide to be the parent is $(3.38 \pm 1.80) \times 10^{-4}$ and $(2.76 \pm 1.47) \times 10^{-4}$, respectively.

4.3.5 *Upper limits for* H_2S_2 *and* S_2H

Based on the four spectra shown in Section 4.1.3, it is possible to derive an upper for S_2H/H_2S and H_2S_2/H_2S during 2014 October. The estimated maximum peak area due to S_2H is 25 ions. Then one has to distinguish two cases, first S_2H is a fragment due to the ionization process in DFMS, second S_2H is present in the coma. For both S_2H and H_2S_2, neither fragmentation pattern nor ionization cross-section is reported in the literature. Thus, local densities were calculated using the fragmentation pattern of C_2H_2 since it has a similar molecular structure while for the ionization cross-section the one of S_2 has been used. Assuming that S_2H is present in the coma, this yields an upper limit for S_2H/H_2S of 1.0×10^{-4}. In case S_2H is solely due to fragmentation of H_2S_2, the limit for H_2S_2/H_2S is 5.7×10^{-4}. The uncertainties in these limits are estimated to be a factor of 10.

4.4 SO/SO_2

Fig. 15 shows the time series of SO/SO_2 between equinox and perihelion. The significant changes in spacecraft attitude and orbit are indicated by the dark and light grey areas (for more details, see Fig. 1). The values reported in the following paragraph have been corrected for the effects of photodissociation and ionization. Between equinox and end of May, the mean value for SO/SO_2 is 0.39 ± 0.01 ($\sigma = 0.11$). During this time, *Rosetta* was sampling evenly summer and winter hemisphere while staying between Sun and comet (phase angle $< 90^\circ$). Between beginning of June and end of July, less data are available and the scatter of SO/SO_2 is about a factor of 6 higher than during the previous period. The mean is 0.59 ± 0.04 ($\sigma = 0.66$) and represents more the SO/SO_2 ratio for the northern latitudes during winter since around 81 per cent of the data were sampled above the northern latitudes. Between the end of July and perihelion, SO/SO_2 reached its maximum with a mean

Table 6. Relative abundances of C_2H_6S in 2014 October relative to H_2S and H_2O, respectively together with the mean value ($\pm 1\sigma$). Since DFMS cannot distinguish between ethanethiol and dimethyl sulphide, two cases were assumed. First, the signal is only due to ethanethiol and second only due to dimethyl sulphide. Systemic uncertainty of up to a factor of 2 (see Section 3.3) and the effect of photodissociation/ionization are not taken into account here.

Time (UTC)	C_2H_6S/H_2S (Ethanethiol)	C_2H_6S/H_2S (Dimethyl sulphide)	C_2H_6S/H_2O (Ethanethiol)	C_2H_6S/H_2O (Dimethyl sulphide)
17.10.2014 11:46	$(3.63 \pm 1.11) \times 10^{-4}$	$(2.97 \pm 1.05) \times 10^{-4}$	$(1.61 \pm 0.42) \times 10^{-6}$	$(1.32 \pm 0.47) \times 10^{-6}$
19.10.2014 17:05	$(3.47 \pm 1.05) \times 10^{-4}$	$(2.84 \pm 0.98) \times 10^{-4}$	$(3.41 \pm 0.89) \times 10^{-6}$	$(2.79 \pm 0.98) \times 10^{-6}$
20.10.2014 08:06	$(6.70 \pm 2.33) \times 10^{-5}$	$(5.48 \pm 0.22) \times 10^{-5}$	$(4.98 \pm 1.23) \times 10^{-7}$	$(4.07 \pm 1.67) \times 10^{-7}$
23.10.2014 11:15	$(5.73 \pm 1.71) \times 10^{-4}$	$(4.69 \pm 1.61) \times 10^{-4}$	$(2.31 \pm 0.60) \times 10^{-6}$	$(1.89 \pm 0.66) \times 10^{-6}$
Mean $\pm 1\sigma$	$(3.38 \pm 1.80) \times 10^{-4}$	$(2.76 \pm 1.47) \times 10^{-4}$	$(1.96 \pm 1.06) \times 10^{-6}$	$(1.60 \pm 0.87) \times 10^{-6}$

Table 7. Overview on the S_2H/H_2S and H_2S_2/H_2S ratios measured in the low-mass protostar IRAS 16293−2422, derived from laboratory studies of ice analogues, and upper limit in 67P during 2014 October.

	S_2/H_2S	S_2H/H_2S	H_2S_2/H_2S
IRAS 16293−2422[a]	$\leq 5.5 \times 10^{-1}$	$\leq 2.0 \times 10^{-2}$	$\leq 1.5 \times 10^{-2}$
Laboratory study[b]	–	15	≤ 25.0
67P upper limit	2.61×10^{-5}	$\leq 1.0 \times 10^{-4}$	$\leq 5.7 \times 10^{-4}$

[a]Martín-Doménech et al. (2016).
[b]Martín-Doménech et al. (2016) derived the ratios from a laboratory study performed by Jiménez-Escobar et al. (2012).

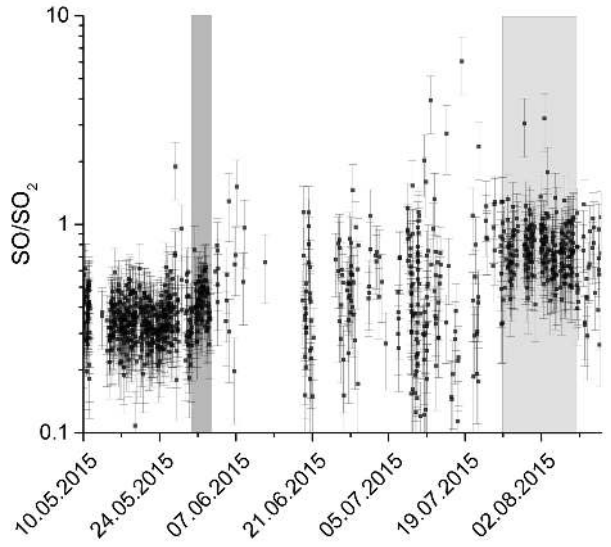

Figure 15. SO/SO_2 ratio between equinox and perihelion. Significant spacecraft attitude changes are indicated by dark grey rectangle for going from phase angle 60° to 90° and with light grey rectangle when *Rosetta* went to 45° south and back to the equator while being in terminator orbit.

value of 0.74 ± 0.02 ($\sigma = 0.37$) while *Rosetta* was going from the equator to −45° latitude and back to the equator. Our SO/SO_2 ratios of 0.4–0.7 measured in 67P are generally somewhat lower than the observed interstellar SO/SO_2 ratios in hot cores, which range from 1 to 10 (e.g. Schöier et al. 2002; van der Tak et al. 2003; Herpin et al. 2009).

4.5 Elemental abundance ratio S/O

A quantity of importance of sulphur chemistry in comets, is the S/O bulk abundance, in order to find out if comets contain their full complement of sulphur or if comets also lack sulphur as do the pre-

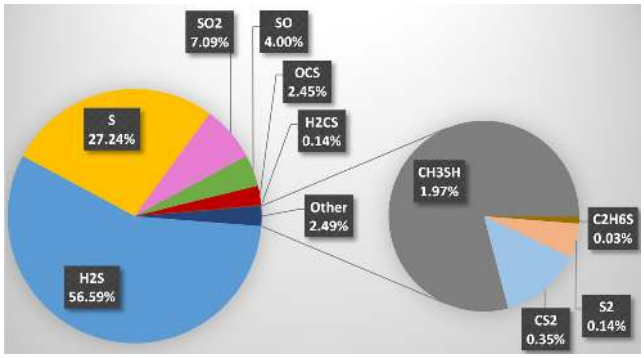

Figure 16. Sulphur-bearing species budget: for H_2S, S, SO, SO_2, OCS, S_2 and CS_2, the assumed bulk values have been used; for CH_3SH the supposed bulk measured at the end of 2016 July is used, while for the remaining species the mean has been used. All values have been corrected for the effect of photodissociation (see Section 4.3.1).

solar dense clouds. In Fig. 16, the relative contributions to the overall sulphur content in the volatile material of the comet are shown. H_2S is the most abundant species and contributes ∼57 per cent to the total sulphur content. The atomic sulphur is surprisingly high with about 27 per cent, whereas S_2 adds only 0.14 per cent of the sulphur. The oxygenated S-bearing species contribute less than 14 per cent and the organo-sulphur species about 2 per cent. If we neglect the minor sulphur-bearing species (e.g. organo-sulphur) and the minor oxygenated species (e.g. alcohols) in the coma, we can calculate the S/O ratio in the volatile material according to

$$\mathrm{S/O} = \frac{n_{\mathrm{H_2S}} + n_{\mathrm{S}} + n_{\mathrm{OCS}} + 2 \cdot n_{\mathrm{S_2}} + n_{\mathrm{SO_2}} + 2 \cdot n_{\mathrm{CS_2}} + n_{\mathrm{SO}}}{n_{\mathrm{H_2O}} \cdot (1.0 + 2 \cdot 0.038) + n_{\mathrm{CO}} + 2 \cdot n_{\mathrm{CO_2}}}, \quad (4)$$

where n_x is the number density of species x. In order to take into account molecular oxygen, the mean value of 3.8 per cent relative to water has been used (Bieler et al. 2015). These data have not been corrected for photodissociation which introduces a bias estimated up to 10 per cent towards perihelion. The overall uncertainty of the obtained S/O value of the measured volatiles is 120 per cent due to the unknown sensitivities of several species.

The resulting S/O ratio between equinox and perihelion is shown in Fig. 17 together with the chondritic and the photospheric value (Lodders 2010), the value for dust at Halley (Jessberger, Christoforidis & Kissel 1988), the mean value between equinox and perihelion of $(1.47 \pm 0.03, \sigma = 1.16) \times 10^{-2}$, the mean between equinox and end of May representing the ice in 67P of $(1.47 \pm 0.05, \sigma = 0.74) \times 10^{-2}$, and the derived total S/O ratio (see Section 5.6).

Unlike H_2S/H_2O, S/O shows considerable variation between equinox and perihelion, which can be explained by the variation in the ratios of the minor sulphur-bearing species to H_2O. However,

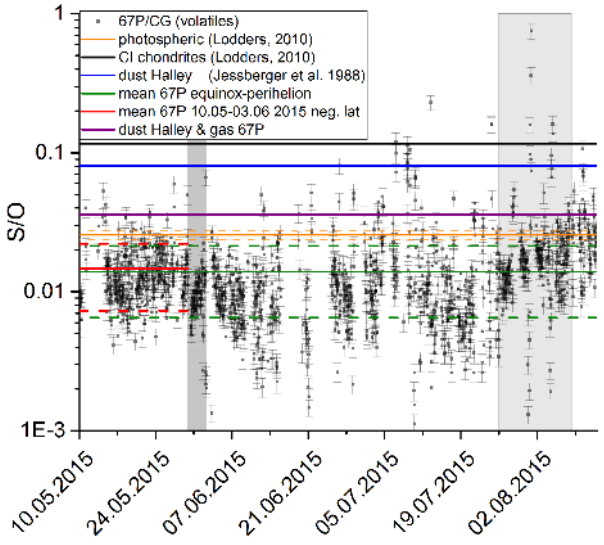

Figure 17. Elemental abundance S/O between equinox and perihelion. Using calculated sensitivities leads in average to a bias of 120 per cent which has not been considered here. Significant spacecraft attitude changes are indicated by dark grey rectangle for going from phase angle 60° to 90° and with light grey rectangle when *Rosetta* went to 45° south and back to the equator while being in terminator orbit.

similar to some of the presented species before, one can divide the time range into three periods. During the first period, S/O is rather constant when *Rosetta* was sampling both hemispheres equally with phase angles <90°. During the second period, *Rosetta* was in terminator orbit, sampling solely the Northern hemisphere and S/O increased by almost a factor of 2. In the third period, when *Rosetta* was going back to southern latitudes and doing the transition from 200 to 300 km, distance to the comet S/O increases slightly compared to bulk. However, the increase is not significant.

5 DISCUSSION

In the following, we discuss (i) how the inventory of sulphur-bearing species compares to measurements in other comets, (ii) what can be learned from the newly detected species, (iii) the implications on radiolysis of H_2S with respect to comets, (iv) why the detection of S_2 is a key measurement for the Solar system formation, (v) how 67P compares to the recent interstellar chemistry model by Woods et al. (2015), and (vi) finally we discuss the elemental abundance S/O of the volatile phase in 67P and estimate the total elemental abundance for 67P.

5.1 Comparison of 67P to other comets

H_2S has been detected in all comets listed in Table 1 and ranges at 1 au from 0.2 per cent in 73P/Schwassmann–Wachmann3/B to 1.5 per cent in C/1995 O1 Hale–Bopp relative to water. Besides H_2S, OCS, SO_2, CS_2, SO and S_2 have been detected in several comets. SO_2 has been seen only in one, namely Hale–Bopp and H_2CS in the comets Hale–Bopp and C/2014 Q2 Lovejoy. In the following, a comparison to those comets is done without considering their dynamical origin since there is no distinct proof linking compositional heterogeneity and dynamical origin. Fig. 18 shows a compilation of the abundances relative to water presented in Table 1 and the results of this work. Compared are the range of different measurements in comets for H_2S, OCS, SO and S_2 (grey rectangle),

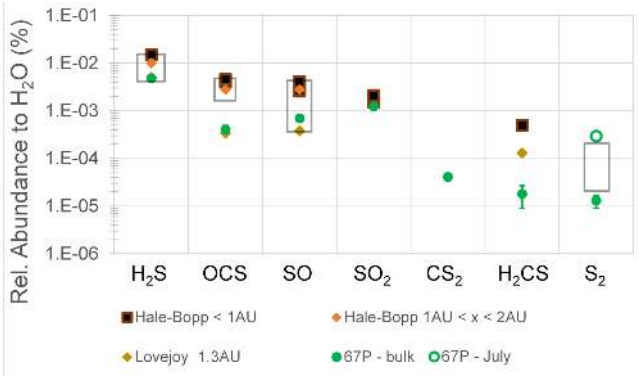

Figure 18. Comparison of abundance for S-bearing species between comets in general (grey rectangle) and assumed bulk ice in 67P (green filled circles). In addition to 67P, all data present for comet Hale–Bopp (black squares and orange rhombus) and C/2014 Q2 Lovejoy (golden rhombus) are shown since both contain a majority of the so far detected S-bearing species. The displayed error bars represent the statistical and methodical uncertainties. However, for all sulphur-bearing species except H_2S, a systematic uncertainty up to a factor of 2 is present due to the usage of a calculated sensitivity (see Sections 3.2 and 3.3) which is not part of the error bar.

comet Hale–Bopp inside 1 au (black square with red line) and between 1 and 2 au (orange rhombus), comet Lovejoy at about 1.3 au (golden rhombus) and the bulk abundance (this work, green circle). CS and CS_2 are not taken into account since CS is not present in the coma of 67P, and the values reported for CS_2 in other comets are deduced from the presence of CS. The relative bulk abundances to water of H_2S, OCS, SO and SO_2 in 67P are comparable with previous measurements in other comets while the value of S_2 between equinox and end of 2015 May is just below the range of other measurements. However, if we compare the perihelion value of S_2 in 67P which include some of the refractory part of S_2, the value in 67P of 0.29‰ is then above the measured range. So far S_2 has been measured in comet C/1996 B2 Hyakutake, C/1999 H1 Lee, C/1999 S4 (LINEAR), C/1983 H1 *IRAS*–Araki–Alcock and 153/2002 C1 Ikeya–Zhang at distances below 1 au; thus, thermal fragmentation and release of refractory S_2 is thought to be more important. However, this is partially countered, as remote sensing probes a much larger distance range around the nucleus, where S_2 then disappears due to photodestruction. It is surprising that SO/H_2O in 67P lays within the range of previous remote sensing measurements, since a considerable fraction of this measured SO is thought to be produced by the photodestruction of SO_2.

5.2 What can be learned from newly detected parent species and the presence of atomic sulphur in the coma of 67/P

It is evident from our measurements that atomic sulphur cannot be accounted for by just electron impact ionization of the sulphur-bearing species inside DFMS or by their photodissociation in the coma. Part of the measured atomic sulphur may be either sputtered or thermally released from the (semi-) refractory part of the sulphur reservoir, the sulphur polymer S_n. According to Woods et al. (2015), significant amounts of atomic sulphur are produced by radiolysis but it is unclear if and how atomic S can survive in the ice. Therefore, the origin of the measured atomic sulphur is unclear, and laboratory experiments are required to see if atomic sulphur can remain in the ice over a long time.

However, organo-sulphur molecules (C_xH_yS) have been detected in other objects outside of the Solar system. The most simple

organo-sulphur molecule H_2CS has been detected in the low-mass protostar IRAS 16293−2422 (Schöier et al. 2002). This detection is of importance for cometary science since this source is thought to be a 'template' source for astrochemistry in a low-mass protostar as the Sun was once (Blake et al. 1994). In addition to H_2CS, the detection of CH_3SH, the second simplest organo-sulphur molecule, has been reported by Majumdar et al. (2016) for the same source.

CH_3SH has also been detected in massive star-forming regions such as SgrB2 close to the galactic centre (Linke, Frerking & Thaddeus 1979; Müller et al. 2016), in the chemically rich massive hot core G327.3−6 (Gibb et al. 2000) and in Orion KL (Kolesniková et al. 2014). In all these sources, the detected molecules are thought to have just sublimated off the icy grains. For IRAS 16293−2422, Majumdar et al. (2016) report a modelled abundance of 4×10^{-9} compared to H_2 for the hot core region. The abundance relative to H_2S can be estimated by taking the abundance of H_2S (compared to H_2) of 9×10^{-8} reported by Schöier et al. (2002). This leads to $CH_3SH/H_2S = 4.4 \times 10^{-2}$ for IRAS 16293−2422, which is a factor of 3 higher than that of 67P at $(1.44 \pm 0.42) \times 10^{-2}$. However, due to the unknown exact sensitivity for CH_3SH with DFMS, the measured CH_3SH/H_2S can be biased by up to a factor of 2, and the interstellar value has a similar overall uncertainty. Consequently, the two measurements can still be consistent.

The presence of C_2H_6S indicates that even more complex organo-sulphur molecules exist. Ethanethiol, one of the two isomers of C_2H_6S, has been detected so far in the hot core of Orion KL by Kolesniková et al. (2014). In addition, they detected CH_3SH and estimated the CH_3SH/C_2H_6S ratio to be about 5 based on the measured column densities. This ratio is similar to that of 11 ± 4 found for 67P. Although absolute sensitivities with DFMS can have a bias of a factor of 2 for species which have not yet been calibrated, the relative sensitivities of the same molecule type are thought to be in the range of 30 per cent. Since these two molecules are similar in structure and differ only slightly in their number of atoms, the above ratio between CH_3SH and C_2H_6S in 67P has an accuracy which makes a comparison with the interstellar result meaningful. The two ratios are surprisingly close, even though Orion KL is a high-mass star-forming region rather than a solar-mass protostar. This may again point to a formation mechanism with grain surface chemistry in the parent cloud followed by incorporation into comets. Overall, ice abundances and grain surface chemistry show many similarities for low- and high-mass protostars (e.g. Herbst & van Dishoeck 2009; Öberg et al. 2011).

5.3 Radiolysis of H_2S

The fact that S_2 was already seen at distances larger than 3 au suggests that it is improbable that S_2 is formed by chemistry in the cometary coma. Densities at that time were very low (Bieler et al. 2015), making collisions among the volatile particles very rare. According to A'Hearn et al. (1983), S_2 could be produced in long-period comets by photolysis from CS_2 and other sulphur-bearing species, but not in short-period comets like 67P. Since 67P loses more than 1 m of its surface on the Southern hemisphere per orbit (Keller et al. 2015) to which depth cosmic rays can hardly penetrate, we would have to observe a decrease of S_2 with time, which we do not. The suggestion that H_2S formed in the dust mantles and was then converted into S_n and other species is also in line with the proposal that O_2 in the comet may have formed by radiolysis (Bieler et al. 2015). Both species, H_2S and O_2, seem to be very well trapped by the matrix in which they were formed and are released only when water actually sublimates, which is at temperatures between 140 and 180 K (Jiménez-Escobar & Muñoz Caro 2011; Mousis et al. 2016). Bieler et al. (2015) have argued that O_2 has to be primordial as the O_2 abundance shows a very good correlation with water, but no dependence on latitude, and also did not change during the orbit of the comet from 3.5 to 1.3 au. Mousis et al. (2016) show that radiolysis was not efficient enough and/or did not last long enough in the solar nebula to produce sufficient O_2 even assuming extreme levels of cosmic rays. The same seems to be true for S_2. For oxygen also, some HO_2 and H_2O_2 were detected at low levels but no O_3 (Bieler et al. 2015). In the case of sulphur, we have very low upper limits for S_2H and H_2S_2 which are always present in laboratory experiments at quite high levels when irradiating H_2S in an H_2O matrix (see Table 7). Contrary to oxygen, we detect S_3 and even S_4 and we also detected a dependence of the S_2 abundance on dust which we attribute to semi-refractory S_2. The very low abundances of the by-products of radiolysis of H_2O and H_2S are a puzzle which is not solved and probably needs more laboratory work. Whereas O_2 could also be due to gas-phase chemistry, at least in warm clouds (Taquet et al. 2016), this pathway does not seem to work for S_n and the puzzle of the missing by-products remains.

5.4 Implication of volatile S_2 on cometary ice

The detection of S_2 being a very volatile species has a very important implication. The photo lifetime of S_2 at 1 au is 250 s by UV photons with a wavelength of 280 nm (De Almeida & Singh 1986). This means that once S_2 is released from the ice, it is destroyed almost immediately. For our measurements at less than 400 km from the comet, it means that more than 50 per cent is lost when we measure at 300 km. However, more importantly, as S_2 was most probably formed in the pre-solar cloud in dust ice mantles, this means that some of these dust ice mantles have survived the formation of the solar nebula and the formation of comets.

In addition to the short photo lifetime of S_2, no shielding effect is expected to be present as abundant molecules such as CO, H_2O and CO_2 do not have any significant absorption bands in this wavelength regime (Tchang-Brillet et al. 1992; Mordaunt, Ashfold & Dixon 1994; Song et al. 2014) and because of its low abundance, S_2 is also not expected to be able to efficiently shield itself from UV photodissociation (unlike, e.g. water; Bethell & Bergin 2009). Therefore, the disc is presumably optically thin for UV photons capable of dissociating S_2. Then, the lifetime of S_2 at 30 au in the disc would be substantially shorter than the formation time of comets.

This means that 67P contains at least some unaltered volatile ice from the pre-solar cloud. This most certainly also precludes clathrates in comets which contain S_2, such as 67P, as described by Mousis et al. (2016). In this paper, the authors claim that amorphous ice could have transformed into crystalline ice around 120–150 K, thus expelling all molecules into the gas phase except O_2 and then later trap them again in clathrates. This contradicts the presence of volatile S_2 which would have been destroyed very quickly after its release.

5.5 Comparison with interstellar models

The relative abundances of the sulphur-bearing species in the coma of comet 67P (Fig. 16) show generally good agreement with the ice mantle model by Woods et al. (2015, their fig. 3) for collapsing cloud models in which cosmic rays are somewhat enhanced and hydrogenation of the accreting species is less than 50 per cent. This model is a follow-up of Esplugues et al. (2014), who investigated the time-dependent sulphur chemistry evolution using a coupled

gas-grain model approach starting with the cloud collapse and condensation of species on to grain surfaces followed by sublimation and subsequent chemical reactions during the formation of the central protostar. The main addition of the Woods et al. (2015) models is the inclusion of the results of the ice photolysis and radiolysis experiments to form refractory sulphur-bearing species.

In interstellar clouds, the ratios of SO and SO_2 with respect to H_2S have attracted significant attention as a potential chemical 'clock' for hot cores. The idea, suggested by Charnley (1997), is that H_2S ice sublimates into the gas and is then gradually converted into SO and SO_2 by high-temperature gas-phase chemical reactions over a period of about 10^5 yr (see also Buckle & Fuller 2003 for low-mass cores). Various studies have pointed out difficulties with this scenario, however (e.g. Viti et al. 2004; Wakelam, Hersant & Herpin 2011). Our conclusion that both SO and SO_2 are parent molecules in cometary ices further strengthens the notion that these ratios are of limited value as a clock.

The average relative bulk abundances for 67P of $H_2S/SO_2/SO$ = 100/13/7 (Table 3) suggest a fairly limited chemical evolution of H_2S to other species. This is furthermore supported by the even lower abundance of carbonyl sulphide and other C-S-bearing species which are generally formed at even later stages in these models (Buckle & Fuller 2003; Jørgensen, Schöier & van Dishoeck 2004).

5.6 Elemental abundance of sulphur

The photospheric value of S/O (Lodders 2010) is about a factor of 1.9 higher than our bulk value during May, but still within the 2σ boundary. In addition, our value just represents the volatile and probably part of the semi-volatile sulphur. The bulk ice value S/O in 67P of $(1.47 \pm 0.05) \times 10^{-2}$ is ∼1.4 lower than the gas-phase value reported for comet Hale–Bopp (Bockelée-Morvan et al. 2000). However, as there is limited information on the uncertainty of this value, the only conclusion that can be drawn is that both 67P and Hale–Bopp are within 2σ boundary photospheric.

There is not yet a S/O value available from the dust mass spectrometer Cometary Secondary Ion Mass Spectrometer (COSIMA) on *Rosetta*. However, at comet Halley S/O in the dust has been measured by the PUMA instrument and yields (8.1 ± 2.8) per cent (Jessberger et al. 1988). According to Geiss (1988), 23 per cent of oxygen is in the refractories with a dust/ice ratio for Halley of 2, whereas for 67P this ratio is 4 ± 2 (Rotundi et al. 2015). We therefore assume that in 67P 47 per cent of the oxygen is in dust. Assuming the same S/O ratio in dust for both comets, we then arrive at a bulk abundance for S/O of 3.6 per cent. This is slightly higher, but certainly within 1σ of the value by Lodders (2010). Some of this may be due to the fact that the semi-refractories are measured in both cases, once as the product of thermal fragmentation in the volatiles, once as part of the dust grains. This means that comet 67P has its full complement of sulphur and therefore we deduce, assuming that the Solar system represents the nominal case, that the apparent sulphur deficit in pre-solar clouds/star-forming regions is due to an observational bias, because the products of radiolysis (the refractory sulphur species in the ice) and ice phase sulphur cannot be detected by remote sensing.

6 CONCLUSIONS

ROSINA/DFMS detected four sulphur-bearing species (S_3, S_4, CH_3SH, C_2H_6S) never seen in comets before in the coma of 67P, and this list is likely not exhaustive! There might be more sulphur-bearing species hidden in the data. The fact that most sulphur-bearing species could be observed over much of the orbit of 67P shows desorption patterns and helps distinguish between species desorbing from ice or dust.

CS, which has been detected in other comets, is most likely not a parent in the coma of 67P but a fragment of OCS and CS_2. The detection of S_2, S_3 and S_4 makes radiolysis of H_2S a very likely process which could well connect the cometary ice to the ISM. If these species were produced in the cloud prior to the formation of the protosun, this would mean that at least part of the ice never sublimated before being incorporated in 67P. This is supported by the fact that there is very volatile S_2 present already at 3 au, which has a very short photo lifetime, thus making its survival in the gas phase of the solar nebula very unlikely.

The field of exoplanet exploration is evolving rapidly thanks to more sophisticated techniques. With this evolution, the question of how to detect life on other planets and star systems gains importance. Comparing a list of bio-signatures recently published by Seager, Bains & Petkowski (2016) reveals that many of the detected sulphur species in comet 67P are defined as such. In addition to the sulphur species 67P also contains O_2 (Bieler et al. 2015), HCN, CH_4 (Le Roy et al. 2015) and glycine (Altwegg et al. 2016) in its coma. However, it is not possible to have life in the cold, primitive environment of a comet. Consequently, one has to be very careful when defining and searching for bio-signatures. Furthermore, the strong links between the comet and the ISM suggest that the involved processes and species are not unique to our Solar system but rather common throughout the Universe.

ACKNOWLEDGEMENTS

ROSINA would not give such outstanding results without the work of the many engineers, technicians and scientists involved in the mission, in the *Rosetta* spacecraft and in the ROSINA instrument team over the last 20 years, whose contributions are gratefully acknowledged. *Rosetta* is a European Space Agency (ESA) mission with contributions from its member states and NASA. We acknowledge herewith the work of the whole ESA *Rosetta* team.

Funding. Work at University of Bern was funded by the State of Bern, the Swiss National Science Foundation and the ESA PRODEX (PROgramme de Développement d'Expériences scientifiques) programme. Work at BIRA-IASB was supported by the Belgian Science Policy Office via PRODEX/ROSINA PEA90020 and 4000107705 and by the F.R.S.-FNRS grant PDR T.1073.14 'Comparative study of atmospheric erosion'. Research at Southwest Research Institute is funded by NASA through JPL contract No.196541. This work has been carried out with the support of the A*MIDEX project (no. ANR-11-IDEX-0001-02) funded by the 'Investissements d'Avenir' French Government programme, managed by the French National Research Agency (ANR). This work was supported by CNES (Centre National d'Etudes Spatiales) grants at LATMOS (Laboratoire Atmosphères, Milieux, Observations Spatiales). Work at the University of Michigan was funded by the US *Rosetta* Project under JPL contract No.1266313. EvD is supported by European Union A-ERC grant 291141 CHEMPLAN.

REFERENCES

A'Hearn M. F., Schleicher D. G., Feldman P. D., 1983, ApJ, 247, L99
Altwegg K. et al., 2016, Sci. Adv., 2, e1600285
Atreya S. K., Mahaffy P. R., Niemann H. B., Wong M. H., Owen T. C., 2003, Planet. Space Sci., 51, 105

Balsiger H. et al., 2007, Space Sci. Rev., 128, 745
Berthelier J.-J., Illiano J.-M., Nevejans D., Neefs E., Arijs E., Schoon N., 2002, Int. J. Mass Spectrom., 215, 89
Bethell T., Bergin E., 2009, Science, 326, 1675
Bieler A. et al., 2015, Nature, 526, 678
Biver N. et al., 1999, AJ, 118, 1850
Biver N. et al., 2000, AJ, 120, 1554
Biver N. et al., 2002, Earth Moon Planets, 90, 5
Biver N. et al., 2006, A&A, 449, 1255
Biver N. et al., 2007, Icarus, 187, 253
Biver N. et al., 2008, LPI Contrib., 1405, 8149
Biver N. et al., 2015, Sci. Adv., 1, e1500863
Blake G. A., van Dishoeck E. F., Jansen D. J., Groesbeck T. D., Mundy L. G., 1994, ApJ, 428, 680
Bockelée-Morvan D. et al., 2000, A&A, 353, 1101
Bockelée-Morvan D. et al., 2001, Science, 292, 1339
Bockelée-Morvan D., Crovisier J., Mumma M. J., Weaver H. A., 2004a, The Composition of Cometary Volatiles. Univ. Arizona Press, Tucson, p. 391
Bockelée-Morvan D. et al., 2004b, Icarus, 167, 113
Boogert A. C. A., Schutte W. A., Helmich F. P., Tielens A. G. G. M., Wooden D. H., 1997, A&A, 317, 929
Buckle J. V., Fuller G. A., 2003, A&A, 399, 567
Charnley S. B., 1997, ApJ, 481, 396
Chen Y.-J. et al., 2015, ApJ, 798, 80
Collings M. P., Anderson M. A., Chen R., Dever J. W., Viti S., Williams D. A., McCoustra M. R. S., 2004, MNRAS, 354, 1133
Cottin H., Fray N., 2008, Distributed Sources in Comets. Springer, New York, p. 179
Crockett N. R., Bergin E. A., Neill J. L., Black J. H., Blake G. A., Kleshcheva M., 2014, ApJ, 781, 114
Crovisier J., Bockelee-Morvan D., Colom P., Despois D., Paubert G., 1991, Icarus, 93, 246
De Almeida A. A., Singh P. D., 1986, Earth Moon Planets, 36, 117
de Sanctis M. C., Capria M. T., Coradini A., 2005, A&A, 444, 605
De Sanctis M. C. et al., 2015, Nature, 525, 500
Dello Russo N., DiSanti M. A., Mumma M. J., Magee-Sauer K., Rettig T. W., 1998, Icarus, 135, 377
Dello Russo N. et al., 2016, Icarus, 266, 152
Eberhardt P., Meier R., Krankowsky D., Hodges R. R., 1994, A&A, 288, 315
Esplugues G. B., Viti S., Goicoechea J. R., Cernicharo J., 2014, A&A, 567, A95
Esposito L. W., Winick J. R., Stewart A. I., 1979, Geophys. Res. Lett., 6, 601
Feldman P. D., Weaver H. A., A'Hearn M. F., Festou M. C., McPhate J. B., Tozzi G.-P., 1999, BAAS, 31, 1127
Ferrante R. F., Moore M. H., Spiliotis M. M., Hudson R. L., 2008, ApJ, 684, 1210
Fougere N. et al., 2016, MNRAS, in press
García-Rojas J., Esteban C., Peimbert M., Costado M. T., Rodríguez M., Peimbert A., Ruiz M. T., 2006, MNRAS, 368, 253
Garozzo M., Fulvio D., Kanuchova Z., Palumbo M. E., Strazzulla G., 2010, A&A, 509, A67
Gautier D., Hersant F., Mousis O., Lunine J. I., 2001, ApJ, 550, L227
Geiss J., 1988, in Klare G., ed., Reviews in Modern Astronomy. Springer-Verlag, Berlin, Heidelberg, p. 1
Gibb E. L., Nummelin A., Bergman P., Irvine W., Whittet D. C. B., 2000, BAAS, 32, 712
Grim R. J. A., Greenberg J. M., 1987, ApJ, 321, L91
Gulkis S. et al., 2015, Science, 347, aaa0709
Hässig M. et al., 2015, Science, 347, aaa0276
Hatchell J., Thompson M. A., Millar T. J., MacDonald G. H., 1998, A&A, 338, 713
Herbst E., van Dishoeck E. F., 2009, ARA&A, 47, 427
Herpin F., Marseille M., Wakelam V., Bontemps S., Lis D. C., 2009, A&A, 504, 853
Howk J. C., Sembach K. R., Savage B. D., 2006, ApJ, 637, 333
Huddleston D. E., Strangeway R. J., Warnecke J., Russell C. T., Kivelson M. G., 1998, J. Geophys. Res., 103, 19887
Huebner W. F., Mukherjee J., 2015, Planet. Space Sci., 106, 11
Irvine W. M., Senay M., Lovell A. J., Matthews H. E., McGonagle D., Meier R., 2000, Icarus, 143, 412
Jenkins E. B., 2009, ApJ, 700, 1299
Jessberger E. K., Christoforidis A., Kissel J., 1988, Nature, 332, 691
Jiménez-Escobar A., Muñoz Caro G. M., 2011, A&A, 536, A91
Jiménez-Escobar A., Muñoz Caro G. M., Ciaravella A., Cecchi-Pestellini C., Candia R., Micela G., 2012, ApJ, 751, L40
Jørgensen J. K., Schöier F. L., van Dishoeck E. F., 2004, A&A, 416, 603
Keller H. U. et al., 2015, A&A, 583, A34
Kim S. J., A'Hearn M. F., 1991, Icarus, 90, 79
Kolesniková L., Tercero B., Cernicharo J., Alonso J. L., Daly A. M., Gordon B. P., Shipman S. T., 2014, ApJ, 784, L7
Le Roy L. et al., 2015, A&A, 583, A1
Lien D. J., 1990, ApJ, 355, 680
Linke R. A., Frerking M. A., Thaddeus P., 1979, ApJ, 234, L139
Llovet X., Salvat F., Bote D., Salvat-Pujol F., Jablonski A., Powell C. J., 2014, NIST Database of Cross Sections for Inner-Shell Ionization by Electron or Positron Impact, Version 1.0, National Institute of Standards and Technology, Gaithersburg, MD
Lodders K., 2010, Astrophysics and Space Science Proceedings, Vol. 16, Principles and Perspectives in Cosmochemistry. Springer-Verlag, Berlin, p. 379
Majumdar L., Gratier P., Vidal T., Wakelam V., Loison J.-C., Hickson K. M., Caux E., 2016, MNRAS, 458, 1859
Martín-Doménech R., Jiménez-Serra I., Muñoz Caro G. M., Müller H. S. P., Occhiogrosso A., Testi L., Woods P. M., Viti S., 2016, A&A, 585, A112
Meier R., A'Hearn M. F., 1997, Icarus, 125, 164
Meier R., Eberhardt P., 1993, Int. J. Mass Spectrom. Ion Process., 123, 19
Moore M. H., Hudson R. L., Carlson R. W., 2007, Icarus, 189, 409
Mordaunt D. H., Ashfold M. N. R., Dixon R. N., 1994, J. Chem. Phys., 100, 7360
Mousis O. et al., 2016, ApJ, 823, L41
Müller H. S. P. et al., 2016, A&A, 587, A92
Nevejans D., Neefs E., Kavadias S., Merken P., Hoof C. V., 2002, Int. J. Mass Spectrom., 215, 77
Öberg K. I., Boogert A. C. A., Pontoppidan K. M., van den Broek S., van Dishoeck E. F., Bottinelli S., Blake G. A., Evans N. J., 2011, in Cernicharo J., Bachiller R., eds, Proc. IAU Symp. 280, The Molecular Universe. Cambridge Univ. Press, Cambridge, p. 65
Owen T., Mahaffy P., Niemann H. B., Atreya S., Donahue T., Bar-Nun A., de Pater I., 1999, Nature, 402, 269
Palumbo M. E., Geballe T. R., Tielens A. G. G. M., 1997, ApJ, 479, 839
Pasek M. A., Milsom J. A., Ciesla F. J., Lauretta D. S., Sharp C. M., Lunine J. I., 2005, Icarus, 175, 1
Pearl J., Hanel R., Kunde V., Maguire W., Fox K., Gupta S., Ponnamperuma C., Raulin F., 1979, Nature, 280, 755
Penzias A. A., Solomon P. M., Wilson R. W., Jefferts K. B., 1971, ApJ, 168, L53
Rodgers S. D., Charnley S. B., 2006, Adv. Space Res., 38, 1928
Rotundi A. et al., 2015, Science, 347, aaa3905
Rubin M., Fougere N., Altwegg K., Combi M. R., Roy L. L., Tenishev V. M., Thomas N., 2014, ApJ, 788, 168
Savage B. D., Sembach K. R., 1996, ApJ, 470, 893
Schöier F. L., Jørgensen J. K., van Dishoeck E. F., Blake G. A., 2002, A&A, 390, 1001
Scholten F., Preusker F., Jorda L., Hviid S., 2015, NASA Planetary Data System and ESA Planetary Science Archive
Seager S., Bains W., Petkowski J. J., 2016, Astrobiology, 16, 465
Smith A. M., Stecher T. P., Casswell L., 1980, ApJ, 242, 402
Snyder L. E. et al., 2001, AJ, 121, 1147
Song Y., Gao H., Chang Y. C., Lu Z., Ng C. Y., Jackson W. M., 2014, Phys. Chem. Chem. Phys., 16, 563
Stein S. E., 2016, in Linstrom P. J., Mallard W. G., eds, "Mass Spectra" by NIST Mass Spec Data Center, NIST Chemistry WebBook, NIST

Standard Reference Database Number 69, Mallard. National Institute of Standards and Technology, Gaithersburg, MD
Taquet V. et al., 2016, MNRAS, in press
Tchang-Brillet W.-U., Julienne P. S., Robbe J. M., Letzelter C., Rostas F., 1992, J. Chem. Phys., 96, 6735
Thomas N. et al., 2015, A&A, 583, A17
Tieftrunk A., Pineau des Forets G., Schilke P., Walmsley C. M., 1994, A&A, 289, 579
Toon O. B., Pollack J. B., Whitten R. C., 1982, BAAS, 14, 743
van der Tak F. F. S., Boonman A. M. S., Braakman R., van Dishoeck E. F., 2003, A&A, 412, 133
van Dishoeck E. F., Blake G. A., 1998, ARA&A, 36, 317
Viti S., Collings M. P., Dever J. W., McCoustra M. R. S., Williams D. A., 2004, MNRAS, 354, 1141
Wakelam V., Hersant F., Herpin F., 2011, A&A, 529, A112
Weaver H., 2000, IAU Circ., 7461
Weaver H. A. et al., 1996, IAU Circ., 6374
Weaver H. A., Feldman P. D., A'Hearn M. F., Arpigny C., Brandt J. C., Stern S. A., 1999, Icarus, 141, 1
Weaver H. A., Feldman P. D., A'Hearn M. F., Arpigny C., Combi M. R., Festou M. C., Tozzi G.-P., 2002, BAAS, 34, 853
Woodney L. M., 2000, PhD thesis, Univ. Maryland
Woodney L. M., McMullin J., A'Hearn M. F., 1997, Planet. Space Sci., 45, 717
Woods P. M., Occhiogrosso A., Viti S., Kaňuchová Z., Palumbo M. E., Price S. D., 2015, MNRAS, 450, 1256
Wouterloot J. G. A., Lingmann A., Miller M., Vowinkel B., Winnewisser G., Wyrowski F., 1998, Planet. Space Sci., 46, 579
Zasowski G., Kemper F., Watson D. M., Furlan E., Bohac C. J., Hull C., Green J. D., 2009, ApJ, 694, 459

APPENDIX A

Table A1. Fraction of initial number density which is expected to be present in the coma at a distance of 200 and 300 km at equinox, end of May and perihelion, respectively.

Species	Non-dissociated fraction per cent			Relative to water per cent			Relative to hydrogen sulphide per cent		
	Equinox 1.66 au	End May 1.55 au	Perihelion 1.24 au	Equinox 1.66 au	End May 1.55 au	Perihelion 1.24 au	Equinox 1.66 au	End May 1.55 au	Perihelion 1.24 au
200 km									
H_2O	100	100	100	100	100	100	103	104	106
H_2S	97	96	94	97	96	94	100	100	100
S	100	100	100	100	100	100	103	104	106
SO	94	93	89	94	93	89	97	97	95
OCS	99	99	98	99	99	98	102	103	104
SO_2	98	98	96	98	98	96	101	101	102
CS_2	72	68	53	72	68	53	75	71	56
CH_3SH	76	72	59	76	73	59	78	75	62
S_2[a]	66	62	48	66	62	48	68	65	50
300 km									
H_2O	100	100	100	100	100	100	105	106	109
H_2S	95	94	91	95	95	92	100	100	100
S	100	100	100	100	100	100	105	106	109
SO	91	90	84	91	90	84	95	95	92
OCS	98	98	97	99	98	97	103	104	106
SO_2	97	96	94	97	96	95	102	102	103
CS_2	60	55	34	60	55	35	63	58	38
CH_3SH	65	60	41	65	60	42	68	64	45
S_2[a]	54	49	33	54	49	33	56	52	36

[a]De Almeida & Singh (1986).

Table A2. Abundance of S-bearing species relative to water. This table is based on table 1 in Rodgers & Charnley (2006) and on table 1 in Bockelée-Morvan et al. (2004a). Please note that most of these values come from remote sensing measurements, for which CS is assumed to be the photodissociation product of CS_2.

Comet	r_H(au)	H_2S	OCS	SO	SO_2	CS	CS_2	H_2CS	S_2	NS
	0.92	–	0.004[14]	0.0026[14]	0.0015[14]	–	–	–	–	–
	0.93	–	–	–	–	–	–	–	–	≥0.0002[15]
	0.95	–	0.0046[13]	–	0.0021[14]	–	–	–	–	–
	0.97	–	–	0.0041[14]	–	–	–	–	–	–
C/1995 O1	∼1	0.015[14]	–	–	–	0.0040–0.01[7]	–	0.0005[22]	–	–
(Hale–Bopp)	1.06	–	0.0028[13]	0.0028[14]	–	–	–	–	–	–
	1.7	0.01[10]	–	–	–	–	–	–	–	–
	2.48	–	–	–	–	0.0009[6]	–	–	–	–
	3.31	–	–	–	–	0.0019[6]	–	–	–	–
	4.79	–	–	–	–	0.006[6]	–	–	–	–
	0.5	<0.0054[2]	–	–	–	–	–	–	–	–
	0.66	0.0077[2]	–	–	–	0.0018[2]	–	–	–	–
	0.84	–	–	–	–	0.0012[2]	–	–	–	–
C/1996 B2	0.89	–	–	–	–	0.000 78[2]	–	–	0.0001[23]	–
(Hyakutake)	0.94	–	–	–	–	0.0011[3]	–	–	–	–
	∼1	0.008[2]	0.001[12]	–	–	0.001[2]	–	–	–	–
	1.24	–	–	–	–	0.000 73[2]	–	–	–	–
	0.93	–	<0.0036[4]	–	–	–	–	–	–	–
	0.97	–	0	–	–	0.000 91[4]	–	–	–	–
C/1999 H1	∼1	<0.0092[4]	–	–	–	0.000 08[4]	–	–	0.000 02[16, 18]	–
(Lee)	1.19	–	–	–	–	0.0006[4]	–	–	–	–
	1.36	–	–	–	–	0.000 79[4]	–	–	–	–
C/1999 S4	0.77	0.0034[5]	–	–	–	0.0012[4]	–	–	–	–
(LINEAR)	∼1	–	–	–	–	–	–	–	0.000 012[25]	–
C/1983 H1 (*IRAS*–Araki–Alcock)	1	–	–	–	–	0.0005[1]	–	–	0.0002[1]	–
C/1989 X1 (Austin 1989c)	1.13	0.0027[11]	–	–	–	–	–	–	–	–
C/1990 K1 (Levy 1990c)	1.32	0.002[11]	–	–	–	–	–	–	–	–
C/2001 A2 LINEAR	1.1	0.0115[19]	–	0.0011[19]	–	0.0004[19]	–	–	–	–
C/1999 T1 (McNaught-Hartley)	1.3	0.0055[19]	–	–	–	0.0008[19]	–	–	–	–
C/2000 WM1 (LINEAR)	1.2	0.0013[19]	–	–	–	0.0005[19]	–	–	–	–
C/2012 S1 (ISON)	0.46	–	0.0016[26]	–	–	–	–	–	–	–
	0.8	–	–	–	–	0.003[24]	–	–	–	–
1P/Halley	1	0.0041[9]	–	–	–	–	–	–	–	–
	1.9	–	–	–	–	0.0005[24]	–	–	–	–
153P/2002 C1	∼1	0.0082[19]	<0.002[16]	<0.0005[19]	–	0.000 67[19]	–	–	–	–
(Ikeya–Zhang)	0.9	–	–	–	–	0.001[17]	–	–	0.000 04[17]	–
122P/de Vico	∼0.67	–	–	–	–	–	–	–	–	–
73P/SW3/B	∼1	0.002–0.004[20]	–	–	–	0.0012–0.0019[20]	–	–	–	–
73P/SW3/C	∼1	0.0016–0.003[20]	–	–	–	0.0008–0.0014[20]	–	–	–	–
9P/Tempel 1 before impact	∼1.6	0.005[21]	–	–	–	<0.0013[21]	–	–	–	–
19P/Borelly	1.36	<0.0045[8]	–	–	–	0.0007[8]	–	–	–	–

[1]Kim & A'Hearn (1991); [2]Biver et al. (1999); [3]Wouterloot et al. (1998); [4]Biver et al. (2000);
[5]Bockelée-Morvan et al. (2001); [6]Weaver et al. (1999); [7]Snyder et al. (2001); [8]Bockelée-Morvan et al. (2004b);
[9]Eberhardt et al. (1994); [10]Biver et al. (2002); [11]Crovisier et al. (1991); [12]Woodney et al. (1997); [13]Dello Russo et al. (1998);
[14]Bockelée-Morvan et al. (2000); [15]Irvine et al. (2000); [16]Bockelée-Morvan et al. (2004a); [17]Weaver et al. (2002);
[18]Feldman et al. (1999); [19]Biver et al. (2006); [20]Biver et al. (2008); [21]Biver et al. (2007); [22]Woodney (2000); [23]Weaver et al. (1996);
[24]Meier & A'Hearn (1997); [25]Weaver (2000); [26]Dello Russo et al. (2016).
Comments: [14]Abundances relative to water are computed assuming [HCN]/[H2O]=2.5E−3.
[20]Please note that the values have been determined graphically.

This paper has been typeset from a TEX/LATEX file prepared by the author.